Response to Reviewers

Dear Editors and Reviewers:

Thank you for your letter and the reviewers' comments regarding our manuscript entitled "Influence of boundary layer structure on air quality in Beijing: Long-term analysis based on self-organized maps" (ID: ACP-2017-1046). These comments have greatly improved the quality of our manuscript and are of important help to our future research. We have addressed the comments carefully and made changes accordingly which we hope satisfying the reviewers. The relevant changes are marked in red in the marked-up manuscript.

Responses to the reviewer's comments:

Reviewer #1:

This manuscript uses an unsupervised machine learning to understand the relationships between boundary layer structure and air quality. The analyses are based on four year measurements, and long-term analysis of measurement is quite limited in China. I would recommend it for publication after some improvements.

Thank you for the positive comments. They encouraged us very much.

Detailed comments are listed below:

1. The authors should carefully check the language and grammar. For example, 'feather' is used many times, but it should be 'feature'. Language problems are in other places as well.

Reply: Thanks for the comment. We checked the language and grammar and re-wrote some sentences in the revised manuscript.

2. Line 63-64: There is no evidence to support this point. Weak surface wind and stable boundary layer stratification do not necessarily mean regional transport cannot happen. Many studies have confirmed the roles of regional transport during haze.

Reply: Thanks for the useful comment. As you said, the transport can occur at any time in the presence of wind, regardless of wind speed. In our previous manuscript, the relative contributions of local accumulation and regional transport were discussed by comparing the ratio of CO/SO_2 under the different stability conditions. However, in the revised process, we found that the ratio of CO/SO_2 may be not an efficient indicator for long-term analysis because SO_2 can be reduced by chemical processes. The previous conclusions based on the ratio of CO/SO_2 were indefinite and therefore removed in the revised paper.

3. The title of 3.2 'Evaluation against meteorological data' is not appropriate. Fig. 3 shows the characteristics of meteorological variables for each classified type

Reply: Thank you for the excellent comments. We merged the meteorological analysis into one section and changed the title in the revised paper. Accordingly, we changed the other sections' title.

"3.1 Self-organized boundary layer meteorology" (Line 157).

"3.2 Implementing the SOM-based ABL classification scheme for urban air quality assessment" (Line 215).

"3.3 Quantifying the contribution of ABL anomaly to typical-month $PM_{2.5}$ air quality" (Line 304).

4. Line 229-239: This explanation is not solid, at least not complete. It is more likely that the increasing stability promotes the accumulation of aerosols, and strong aerosol-radiation interactions inhibit photochemistry.

Reply: Thanks for the useful comment. We explained the response of O_3 to different near-surface stability from both physical and chemical perspectives in the revised paper.

"However, increasing atmospheric stability has the opposite effect on near-surface O_3 concentrations. Since aerosols can absorb and reflect solar radiation and thereby inhibit the photochemical production of O_3 (Gao et al., 2016;Kaufman et al., 2002), the lowest O_3 concentration is observed in Node 9. In addition, considering that ozone is mainly produced in the upper ABL, near-surface O_3 should be strongly modulated by down-mixing processes (Tang et al., 2017b;Tang et al., 2017a). In this light, the varying daytime O_3 peaks across the ABL types can be partly attributed to the various magnitudes of vertical mixing. This is supported by daytime BLH. As have shown in Fig. 4, the daytime BLH is highest in Node 1, followed by Node 7, Node 3 and the lowest in Node 9. Such ordering is generally consistent with the daytime O_3 peaks in these types. Due to the persistent down-mixing caused by strong wind shears, the near-surface O_3 remains a relatively high nocturnal concentration (e.g. about 45 $\mu g/m^3$ in winter) in Node 1. In contrast, the stable nocturnal conditions (e.g., Nodes 9, 7 and 3) are commonly associated with low O_3 concentration (e.g. about 16 $\mu g/m^3$ in winter) due to the lack of vertical mixing, as well as the strong chemical titration by NO emitted from vehicles." (Lines 271-282)

Reviewer #2:

General comments

The paper deals with the influence of boundary layer structure on air quality using 4-year observations. The article presented very interesting study between air pollutants and meteorology, and the study built on very good meteorological measurements data. The paper is certainly worth of publishing as the study itself is extremely interesting. However, some improvements/corrections are suggested.

Thank you very much for the positive comments. We have addressed each of the concerns you've brought up here through our responses below.

Specific comments

1. The title should be modified. Throughout the manuscript, I haven't found the description concerning the calculation of the BLH. Therefore, the title using boundary layer structure is not exactly correct. Maybe atmospheric stability or boundary layer meteorology are much better. In addition, 4-year is not long-term for the observation period. In section 3.4, the authors also discussed the impact of the aerosols on BLH. However, the title just represented the influence of boundary layer meteorology on air quality. I suggest removing section 3.4 or please revise the title correspondingly.

Reply: Thanks for the useful comments. We changed the title in the revised paper. In addition, according to your suggestion, we removed section 3.4 in the revised paper.

"Self-organized classification of boundary layer meteorology and associated characteristics of air quality in Beijing" (Lines 1-2)

2. The radiosondes the authors used mainly represent the stable condition of the boundary layer. However, the air pollutants were observed in the whole day. Especially, the AOD data were just observed during the daytime. As well known, the boundary layer height will develop rapidly during the daytime. Lacking of the daytime observations of boundary layer structures, how about the creditability of the relationship of air pollutants and boundary layer meteorology?

Reply: Thanks for the excellent comments. We estimated the daytime boundary layer height (BLH) with parcel method to detect the boundary layer development after sunrise in the revised manuscript. In general, the daytime boundary layer heights are relatively flat after an extremely stable night, reflecting an insufficient space for vertical mixing in the day. These BLH results together with the classified ABL types jointly supported the analysis on the relationship of air pollutants and boundary layer meteorology.

“To detect the boundary layer development after sunrise, daytime boundary layer height (BLH) is estimated with parcel method (Holzworth, 1964, 1967), i.e., intersecting each day’s 08:00 radiosonde potential temperature (θ) profile at Beijing Observatory with each hour’s (from 09:00 to 15:00) surface θ values, which are calculated from surface air temperature observations. As shown in Fig. 4, the BLH on the days following a strong stable night (i.e., Node 1) is relatively flat, reflecting an inadequate development of daytime boundary layer. Similarity, Node 3 is also followed by a flat daytime BLH variation. The maximum BLH in these two types are lower than 900 m, indicating a limited space for vertical mixing in the day. In contrast, the afternoon BLH in Node 7 can reach up to 1100 m; this mixing depth is conducive to dilute the pollutants accumulated in the previous night. In Node 1, the convective boundary layer develops well, and its maximum height on average exceeds 1500 m, far higher than the values in other types.” (Lines 201-210)

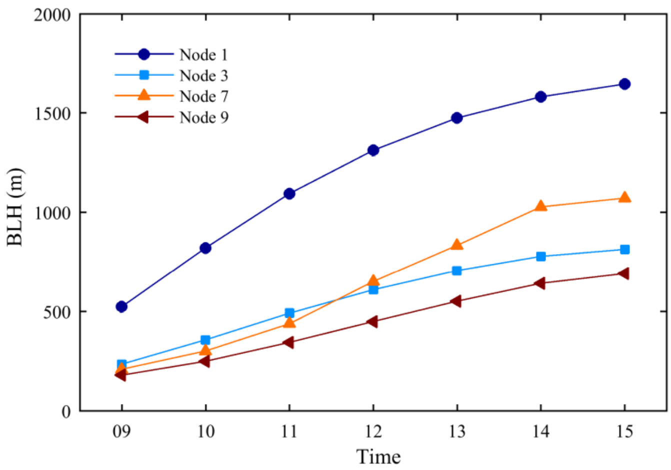

Figure 4. Daytime boundary layer height (BLH) estimated for the four typical ABL types (i.e., Nodes 1, 3, 7 and 9).

3. The instruments of US Embassy for PM are not the same as the MEP. Do you consider the differences?

Reply: Thanks for the comment. The $PM_{2.5}$ values in the two different dataset showed high consistence. We clarified it in the revised paper.

“The mass concentrations of atmospheric pollutants (including $PM_{2.5}$, O_3, NO_2, SO_2 and CO) over Beijing during the period from 2013 to 2017 are obtained from the Ministry of Environmental Protection of the People’s Republic of China (http://datacenter.mep.gov.cn/). In addition, hourly $PM_{2.5}$ measured at the Beijing US Embassy (http://www.stateair.net/) are also used in this study. The

$PM_{2.5}$ values in the two datasets show a well consistence with a mean correlation coefficient of 0.94. The mean hourly standard error of $PM_{2.5}$ across sites changes little from 12.6 to 12.9 after the inclusion of US Embassy.” (Lines 112-117)

4. For the boundary layer meteorology, potential virtual temperature and Richardson number are much better indicators to do the SOM analysis. Why the authors using temperature to do the SOM analysis? I suggest using potential virtual temperature to do the classification of different nodes.

Reply: This excellent comment is highly appreciated. We used virtual potential temperature to perform the classification of boundary layer meteorology in the revised manuscript.

“We construct a 3 × 3 SOM matrix for daily virtual potential temperature deviation profiles, and the self-organized output shown in Fig. 1 represents nine ABL types (i.e., SOM nodes).” (Lines 159-160)

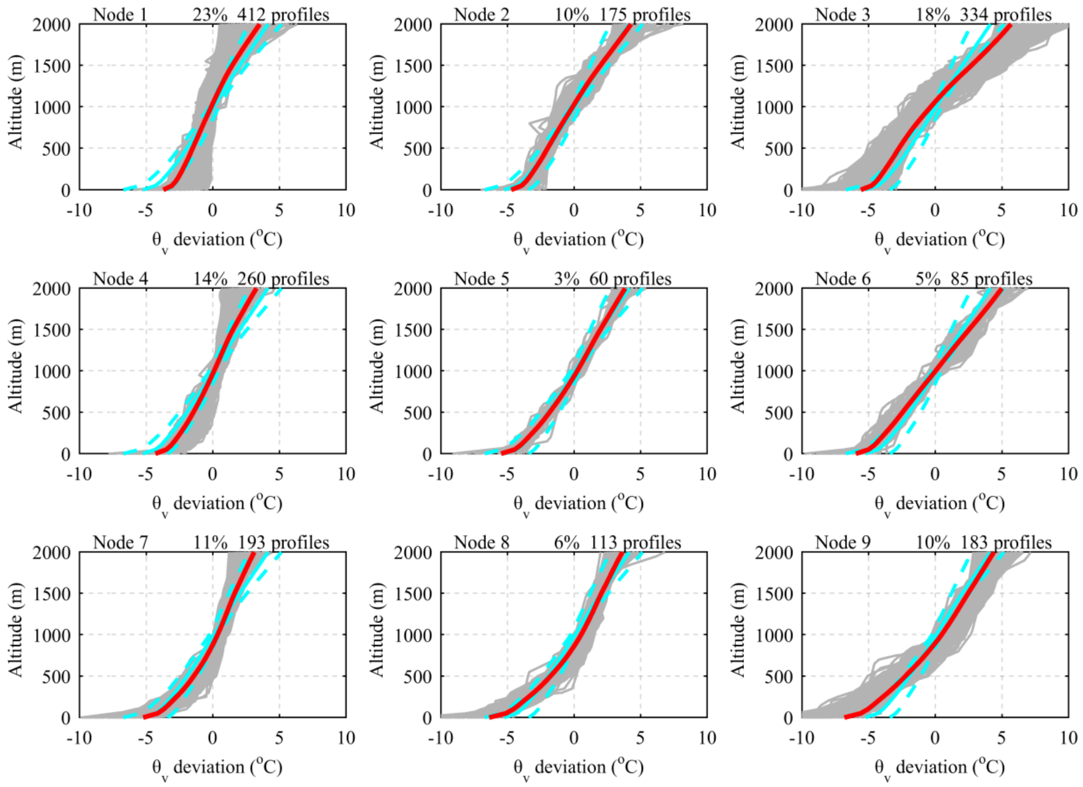

Figure 1. The 3 × 3 SOM output for radiosonde-based virtual potential temperature (θ_v) deviation profiles observed at the Beijing Observatory. SOM nodes are shown in red, with the corresponding individual profiles in grey. For reference, the overall average θ_v deviation profile and 25th and 75th percentile profiles are shown in cyan. The top-right shows the occurrence cases and frequency of each SOM node.

5. How to evaluate atmospheric stability? Do you have the quantitative basis? Node 3 represents slow wind, high humidity and more stable than node 7.

Reply: Thanks for the useful comment. We used the virtual potential temperature gradient profile to quantify the atmospheric stability at different heights (the larger gradient suggests the stronger stability) in the revised paper. We discussed the atmospheric stability throughout the ABL. For Node 3, it represents a strongest stability in the upper ABL compared to other nodes.

"Figure 3 displays the average profiles of wind speed, relative humidity, virtual potential temperature gradient according to the ABL types…" (Lines 181-194)

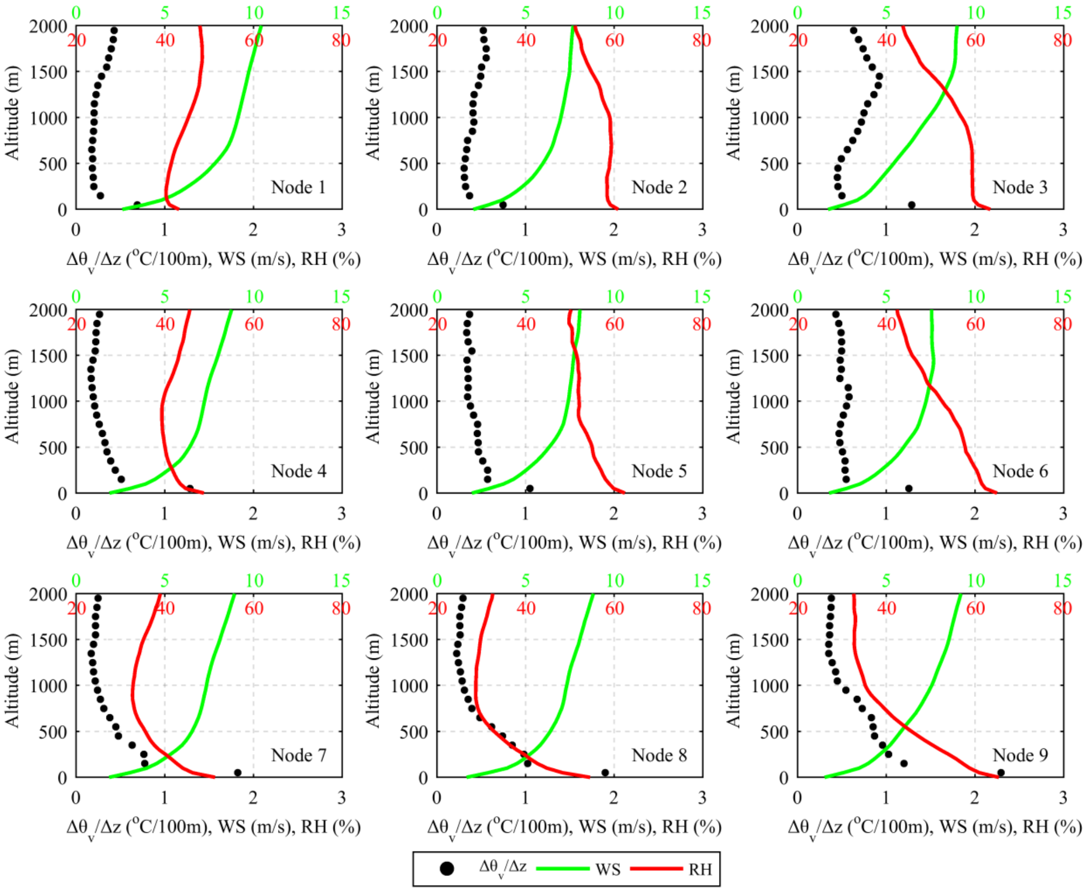

Figure 3. Profiles of average wind speed (WS), relative humidity (RH) and virtual potential temperature gradient ($\Delta\theta_v/\Delta z$) corresponding to individual ABL types (i.e., SOM nodes) at the Beijing Observatory. The black, green and red labels of the horizontal axis correspond to $\Delta\theta_v/\Delta z$, WS and RH, respectively.

6. Because emissions are different in different seasons, I suggest discussing the concentrations of air pollutants in different nodes for each season.

Reply: Thanks for the useful comments. We discussed the concentrations of air pollutants in different nodes separately by seasons, and therefore re-wrote the results in the section 3.2 of the revised paper. (Lines 215-302)

In addition, to increase the sample size, we included the observations in 2017 into analysis in the revised paper. (Lines 94-95 and Lines 112-115)

7. For the boundary layer ozone analysis, please refer Tang et al., 2017a, 2017b.

Reply: Thanks for the comments. We read the two papers carefully and referred them in our boundary layer ozone analysis.

"In addition, considering that ozone is mainly produced in the upper ABL, near-surface O_3 should be strongly modulated by down-mixing processes (Tang et al., 2017b;Tang et al., 2017a). In this light, the varying daytime O_3 peaks across the ABL types can be partly attributed to the various magnitudes of vertical mixing."(Lines 273-276)

Technical comments

1. Line 48. Beijing has two directions adjacent to mountains. The west one is Tai hang Mountains and two north one is Yan Mountains.

Reply: We corrected it in the revised manuscript.

"Beijing, the capital of China, is geographically located at the northwestern border of the Great North China Plain. This city is surrounded by the Yan Mountains to the north and the Taihang Mountains to the west, with the Bohai Sea to the 160 km southeast (Fig. 1)."(Lines 48-50)

2. Line 56. Ground-based remote sensing.

Reply: We corrected it in the revised paper.

"In addition, numerous intensive ABL measures were conducted using other approaches such as mooring boats, airplane, and ground-based remote sensing (Tang et al., 2015;Zhu et al., 2016;Zhang et al., 2009;Hua et al., 2016)." (Lines 60-62)

3. The second paragraph in the introduction section is too long. Please separate it.

Reply: We separated the second paragraph in the revised paper. (Lines 48-68)

4. Section 3.3 is too long, please use subtitle to separate it into several small parts.

Reply: Thanks for the comments. We shorten this section in the revise process and therefore did not use subtitle in the revised paper. In this section, we removed the discussion about local contribution derived from ratio of CO/SO_2. Considering SO_2 are chemical reactive, the chemical process can disrupt the analysis of relative contribution of local accumulation and regional transport.

Other changes:

1、To reflect more daytime concentration after the different stability nights, the daily concentration is performed afternoon-to-afternoon (15:00 h-15:00 h) in the revised paper. In the previous manuscript, the daily concentration was calculated from noon-to-noon (12:00 h-12:00 h).

2、We included the observations in 2017 into analysis in the revised paper. Some according change occurred in the section 3.3 (Quantifying the contribution of ABL anomaly to typical-month $PM_{2.5}$ air quality). Particularly, the results from the meteorology-to-environment method had some difference after the inclusion of observations in 2017. Given that, we updated the results in the revised manuscript.

3、We excluded PM_{10} in the revised paper because to a large extent its characteristics can be represented by $PM_{2.5}$.

~~Influence of boundary layer structure on air quality in Beijing: Long-term analysis based on self-organizing maps~~

Self-organized classification of boundary layer meteorology and associated characteristics of air quality in Beijing

Zhiheng Liao[a], Jiaren Sun[a, b]*, Jialin Yao[c], Li Liu[a], Haowen Li[a], Jian Liu[a], Jielan Xie[a], Dui Wu[d], Shaojia Fan[a]*

[a] School of Atmospheric Sciences, Sun Yat-sen University, Guangzhou, Guangdong, China;

[b] South China Institute of Environmental Sciences, Ministry of Environmental Protection of the People's Republic of China, Guangzhou, Guangdong, China;

[c] Weather Modification Office of Shanxi Province, Taiyuan, Shanxi, China;

[d] Institute of Mass Spectrometer and Atmospheric Environment, Jinan University, Guangzhou, Guangdong, China.

* Address correspondence to S. Fan or J. Sun, School of Atmospheric Sciences, Sun Yat-sen University, Guangzhou, Guangdong, China. Telephone: +86 020 8411 5522.

E-mail: eesfsj@mail.sysu.edu.cn (S. Fan); sunjiaren@scies.org (J. Sun).

Abstract

Self-organizing maps (SOMs; a ~~feather~~feature-extracting technique based on an unsupervised machine learning algorithm) are used to classify ~~the~~ atmospheric boundary layer (ABL) meteorology ~~types~~ over Beijing ~~by~~ through detecting topological relationships among the ~~4~~5-year (2013–~~2016~~2017) radiosonde-based virtual potential temperature– profiles. The ~~resulting~~ classified ~~ABL types~~ABL types are then examined in relation to near-surface ~~air quality, including surface~~ pollutant ~~concentrations~~ concentrations ~~and columnar aerosol properties,~~ to understand the ~~regulating~~ modulation effects of the changing ~~different ABL~~ABL –meteorology~~structures~~ on Beijing's air quality. ~~The SOM provides n~~Nine ABL types (i.e., SOM nodes) are obtained through SOM classification technique, and each ~~type is~~ is characterized ~~by~~ with distinct dynamic and thermodynamic conditions. In general, the self-organized ABL types are able to distinguish between high and low loadings of near-surface pollutants. The average concentrations of $PM_{2.5}$, NO_2 and CO dramatically increased from the near neutral (i.e., Node 1) to strong stable conditions (i.e., Node 9) during all seasons except summer. Since extremely strong stability can isolate the near-surface observations from the influence of elevated SO_2 pollution layers, the highest average SO_2 concentrations are typically observed in Node 3 (a layer with strong stability in the upper ABL) rather than Node 9. ~~On average, SO_2, NO_2, CO, PM_{10} and $PM_{2.5}$ increase 120–220 % from a near neutral (i.e.,~~

~~node 1) to strong stable condition (i.e., node 9).~~ In contrast, near-surface O_3 shows an opposite dependence on atmospheric stability, with the lowest average concentration in Node 9. ~~The ABL controls on diurnal cycles of pollutants are as follows: (1) elevated inversion enhances the afternoon baseline; and (2) surface inversion improves the evening increment. Comparing the CO/SO_2 ratios for the different ABL types demonstrates that the local contribution increases with enhanced static stability near the ground, and it is the stable ABL stratification rather than weak surface wind that confines the regional contribution. Due to regional transport, node 3 (dominated by elevated inversion with high relative humidity) corresponds to the most severe columnar aerosol pollution, characterized by the highest optical depth (1.22) and volume concentration (0.30 μm^3/μm^2). The larger aerosol radiative forcing (ARF) within the atmosphere (> 60 W/m^2) in nodes 3, 6 and 9 is likely to strengthen the atmospheric stability and thus induce a positive feedback loop for causing high surface pollution.~~ Analysis of three typical pollution ~~period~~ months (i.e., January 2013, December 2015 and December 2016) suggests that the ABL types are the primary drivers of day-to-day variations in Beijing's air quality. Assuming a fixed relationship between ABL type and $PM_{2.5}$ loading for different years, the relative (absolute) contributions of the ABL anomaly to elevated $PM_{2.5}$ levels are estimated to be 58.3 % (44.4 μg/m^3) in January 2013, 46.4 % (22.2 μg/m^3) in December 2015, and 73.3 % (34.6 μg/m^3) in December 2016~~65.8 % (46.2 μg/m^3) during January 2013, 46.7 % (20.2 μg/m^3) during December 2015, and 94.6 % (35.3 μg/m^3) during December 2016~~.

1 Introduction

The atmospheric boundary layer (ABL) is the section of atmosphere that responds directly to the flows of mass, energy and momentum from the earth's surface (Stull, 1988). Since most air pollutants are emitted or chemically produced within this layer, its evolution plays an important role in transport~~The atmospheric boundary layer (ABL) is the section of atmosphere that responds directly to the flows of mass, energy and momentum from the earth's surface, characteristically at timescales of an hour or less (Stull, 1988)~~, dispersion and deposition of air pollutants~~. Most air pollutants are emitted or chemically produced within this layer and its evolution plays an important role in determining the dispersive and chemical properties of pollutants~~ (Chen et al., 2012;Fan et al., 2008;Whiteman et al., 2014;Platis et al., 2016;Wolf et al., 2014;Wu et al., 2013). The ABL structure is determined by complex interactions between atmosphere static stability and those mechanical processes (such as wind shear from synoptic or terrain-induced flows) (Stull, 1988;Chambers et al., 2015b). These processes can operate at a variety of different heights and temporal scales, and their dominance may vary considerably with height and time at any given location (Salmond and McKendry, 2005). This makes it very difficult to observe and predict the transport and diffusion of air pollutants within the ABL (Chambers et al., 2015b;Chambers et al., 2015a), particularly in those complex-terrain regions such as Beijing.~~(Stull, 1988)Therefore, characterizing typical ABL conditions associated with high pollution levels helps to better understand the role of ABL in governing the transport and distribution of pollutants in the atmosphere.~~

Beijing, the capital of China, ~~is suffering serious air pollution problems. This city~~ is geographically ~~geographically~~ located at the northwestern border of the Great North China Plain. This city~~ and has~~ is surrounded by the Yan Mountains to the north and the Taihang Mountains to the west~~three directions that are adjacent to mountains.~~, with~~–~~ the Bohai Sea to the 160 km southeast (Fig. 1). Under favorable weather conditions (e.g., stagnant weather), ~~The closest coast from the city of Beijing is the Bohai Sea, which is 160 km southeast of the city. T~~terrain-related circulations can ~~therefore~~ be well developed over Beijing and its surroundings~~ under favorable weather conditions~~, leading to a complex ABL~~ ABL thermodynamic~~ structure, which is thought to substantially affect Beijing's ~~Beijing's~~ air quality (Hu et al., 2014;Miao et al., 2017;Ye et al., 2016;Gao et al., 2016;Xu et al., 2016). With high emissions of air pollutants from anthropogenic sources, Beijing is suffering serious air pollution problems and the pollution can be even more severe when southwesterly and southeasterly winds prevail within the ABL (Chen et al., 2008;Ye et al., 2016;Zhang et al., 2014;Zhang et al., 2012a).

Several studies ~~used tower-based observations to~~ investigated the interactions between ~~boundary layer~~ABL meteorology~~dynamics~~ and air ~~pollution formation~~quality in Beijing using tower-based observations ~~–~~(Sun et al., 2013;Sun et al., 2015;Guinot et al., 2006;Guo et al., 2014). However, the results are not ideal because the tower-based observations~~they~~ have a low observational height (325 m). In addition, n~~N~~umerous intensive ABL measures were conducted using other approaches~~,~~ such as mooring boats, airplane, and ground-based remote sensing (Tang et al., 2015;Zhu et al., 2016;Zhang et al., 2009;Hua et al., 2016). ~~However, s~~Since these approaches are complex, expensive and labor intensive, they are often restricted to the duration of specific research campaigns and hence their results may be considered 'unrepresentative'. Overall, the existing knowledge of linkages between ABL meteorology~~structure~~ and air quality in Beijing is drawn largely from either low observational height or short observational duration~~. Due to the lack of long-term effective observations~~; therefore, the common patterns of the ~~influence~~ influence of the changing ~~ABL~~ ABL structures on Beijing's air quality remains ~~relatively unclear~~unclear and need to be further studied (Quan et al., 2013;Miao et al., 2017;Guo et al., 2014).~~ For example, many case studies (Jia et al., 2008;Zheng et al., 2015;Hua et al., 2016;Li et al., 2016) claimed that rapid growth of PM$_{2.5}$ in Beijing is mainly attributable to the regional transport of the polluted air mass. This view is occasionally questionable, as it is known that the polluted episodes tend to occur with a weak surface wind and stable boundary~~

~~layer stratification, which are unfavorable for transport (Zhu et al., 2016;Tang et al., 2015). Given these uncertainties, there is an urgent need to investigate and determine the common patterns of ABL structure influence on Beijing's air quality.~~

~~On the other hand~~Meanwhile, the ~~long-term~~routine radiosondes are not being fully utilized to investigate urban pollution issues. The advantage of radiosondes over the other approaches seems to be their length, which usually spans several decades. For a long time, it was challenging to reduce the wealth of radiosonde data~~sets~~ to characterize the ABL structure, and therefore, radiosondes remained ~~in~~ a very limited use in case studies (Ji et al., 2012;Zhao et al., 2013;Gao et al., 2016). Recently, self-organizing maps (SOMs; a ~~feather~~feature-extracting technique based on an unsupervised machine learning algorithm) (Kohonen, 2001) were introduced to investigate the ABL thermodynamic structure, indicating the capabilities of SOMs in ~~feather~~ feature extraction from a large dataset of the ABL measurements (Katurji et al., 2015). In fact, the SOM has ~~become~~ an increasing~~ly popular~~ application in atmospheric and environmental sciences during the past several years (Jensen et al., 2012;Jiang et al., 2017;Gibson et al., 2016;Pearce et al., 2014;Stauffer et al., 2016), including a radiosonde-based~~first~~ application ~~of routine radiosondes~~ in South Africa (Dyson, 2015). However, there is thus far no SOM application in air pollution-related ABL structure research. It is expected ~~that~~ such a new analytical approach can tap the potential of routine radiosondes to ~~better~~ reveal ~~understand urban~~the ~~air pollution~~ABL mechanism of air pollution in Beijing.

~~In this study, a long-term analysis regarding~~This study investigates the influence of ABL ~~structure~~ meteorology on Beijing's air quality ~~is performed~~ based on the SOM application ~~of SOMs~~ to ~~4~~ 5 years (2013–~~2016~~2017) of routine meteorological radiosonde~~ measurement~~s. First, we use t~~T~~he SOM~~ is first used~~ technique to classify the state of ABL through detecting topological relationships among the radiosonde-based virtual potential temperature profiles~~vertical temperature profiles for identifying predominant ABL types~~ (see section 3.1). Then, ~~A selection of climatological observations is then subdivided according to the SOM-based ABL classification (see section 3.2). Finally~~we~~, we~~ provide a visual insight into ~~air quality~~near-surface pollutant variations ~~(including surface pollutant concentrations and columnar aerosol properties)~~ under various ABL ~~conditions~~ types and discuss the potential physical mechanisms behind their relationships (see section 3.~~3~~2–3.~~5~~3). It is expected that such an association between air quality and ABL type could provide local policy makers with useful information for improving the predictions of urban air quality.

2 Materials and methods

2.1 Data preparation and preprocessing

The recent 5-year (2013–2017) r~~R~~adiosonde data observed at the Beijing Observatory (39.81°N, 116.48°E, WMO station number 54511) were collected from the University of Wyoming (http://weather.uwyo.edu/). ~~The data cover the recent 4-year period from 2013 to 2016.~~ The radiosondes were ~~Beijing Observatory~~ launched~~s a routine radiosonde~~ twice a day (08:00 and 20:00 ~~Beijing~~ Local Time ~~(BJT)~~, corresponding to the morning and evening, respectively) and ~~provides~~ provided atmospheric sounding data (profiles of temperature, relative humidity, wind speed, etc.) at the mandatory pressure levels (e.g., surface, 1000, 925, 850, 700 hPa) and additional significant levels. In addition, the hourly near-surface meteorological parameters (including temperature, wind speed and relative humidity, etc.) in 2013–2016 ~~are~~were collected from the Beijing Meteorological Bureau.

~~(Li et al., 2012)In addition, the hourly near-surface meteorological parameters (including temperature, wind speed and relative humidity) are also collected from the Beijing Meteorological Bureau.~~

We chose the 2000 m above ground level ~~(AGL)~~ as the upper limit of the ABL based on a number studies investigating the ABL height over Beijing or North China (Tang et al., 2016;Guo et al., 2016;Miao et al., 2017). This height ~~exceeds~~ exceeded the top of the ABL ~~height~~ in most cases, and therefore, most ABL processes influencing the near-surface air quality ~~are~~ were included in the analysis herein. In our study period, the average number of data points in radiosonde profiles was 3.7 below 500 m and 10.1 below 2000 m. Despite the coarse resolution, the profile shapes were enough for SOM technique to classify the state of ABL. Previous radiosonde-based study indicated that surface temperature inversions occur frequently in the eastern China (Li et al., 2012), suggesting that all of the two-time radiosondes mainly represent the nocturnal stable ABL. ~~We classify the daily ABL types using the SOM algorithm.~~ To keep a whole night, the daily ABL~~vertical~~ profiles ~~are~~ were composited from the ~~radiosonde measurement~~radiosondes at 20:00 and 08:00 of the next day.~~In addition, the hourly near-surface meteorological parameters (including temperature, wind speed and relative humidity) are also collected from the Beijing Meteorological Bureau.~~

The mass concentrations of atmospheric pollutants (including ~~SO_2, NO_2, CO, O_3, PM_{10} and~~ $PM_{2.5}$, O_3, NO_2, SO_2 and CO) over Beijing during the period from 2013 to ~~2016~~ 2017 are obtained from the Ministry of Environmental Protection of the People's Republic of China (http://datacenter.mep.gov.cn/). In addition, hourly $PM_{2.5}$ measured at the Beijing US Embassy (http://www.stateair.net/) are also used in this study. The $PM_{2.5}$ values in the two datasets show a well consistence with a mean correlation coefficient of 0.94. The mean hourly standard error of $PM_{2.5}$ across sites changes little from 12.6 to 12.9 after the inclusion of US Embassy. Hourly concentrations are calculated for the Beijing urban area by averaging concentrations from nine urban sites (including Dongsi, Guanyuan, Tiantan, Wanshouxigong, Aotizhongxin, Nongzhanguan, Gucheng, Haidianwanliu and US Embassy). T~~To maintain consistency with ABL classification, t~~he daily pollutant concentration is then performed ~~from~~ afternoon-to-afternoon (15~~2~~:00 h–15~~2~~:00 h), in order to include one whole night in each 24-h period.

~~In addition to near-surface observations, columnar aerosol parameters (including aerosol optical depth (AOD), Ångström exponent (AE), single scattering albedo (SSA), volume particle size distribution (d*V*/dln*R*), aerosol radiative forcing (ARF) and so on) are also collected from the AERONET Beijing (39.98°N, 116.38°E) and Beijing-CAMS (39.93°N, 116.32°E) sites. The level-2.0 quality-assured columnar aerosol data from 2013 to 2016 are downloaded from the AERONET data archive (http://aeronet.gsfc.nana.gov). The size distribution is retrieved in 22 logarithmically equidistant bins in a range of sizes from 0.05 to 15 μm through a combined spherical and spheroid particle model (Dubovik and King, 2000;Dubovik et al., 2006).~~

2.2 Self-organizing maps technique

The SOM is thought to be an ideal tool for ~~feather~~feature extraction because the input data are treated as a continuum without relying on correlation, cluster or eigenfunction analysis (Liu et al., 2006). Since Kohonen (1982) first proposed SOM, it has been widely used for data downscaling and visualization in various disciplines (Jensen et al., 2012;Katurji et al., 2015;Dyson, 2015;Stauffer et al., 2016;Pearce et al., 2014;Jiang et al., 2017). In this study, the SOM is introduced to classify the ABL ~~structures~~types through detecting topological relationships among the 5-year (2013–2017) radiosonde-based virtual potential temperature profiles. Since the SOM is sensitive to the virtual potential temperature value, the deviation profiles, which are determined by subtracting the mean virtual potential temperature of each profile from each level, are used as the SOM input.~~We use the code from the MATLAB SOM Toolbox, which is freely available from http://www.cis.hut.fi/projects/somtoolbox/.~~

The training of SOM is an unsupervised, iterative procedure, and the result is a matrix of nodes (i.e., types) that represent the input data. The following provides a simple introduction about the SOM algorithm, and the details can be found in Kohonen (2001). ~~SOM training is an unsupervised, iterative procedure, and the result is a matrix of nodes (i.e., types) that represent the input data.~~ To learn from the input data, every SOM node has a parametric reference vector with which it is associated, and these reference vectors are randomly generated. After initialization of the reference vectors, a stochastic input vector is compared to every reference vector, and the closest match, named the best-matching unit, is determined by the smallest Euclidean distance. Each reference vector is then updated so that the best-matching unit and its neighbors become more like the input vector. Whether or not a reference vector learns from the input vector is determined by the neighborhood function. Only reference vectors that are topologically close enough to the best-matching unit will be updated according to the SOM learning algorithm.

~~To exclude the influence of actual temperature values, temperature deviation profiles, which are determined by subtracting the mean temperature of each profile from each level in the profile, are used as the SOM input in this study.~~ The first step of SOM training is to determine a matrix size of nodes for initializing the reference vectors. This step is performed subjectively and depends on the degree of generation required (Lennard and Hegerl, 2015). We test several SOM matrixes, and finally select a 3 × 3 matrix, because it captured unique profiles without the profiles being too general as with a smaller matrix, or being too similar as with a larger matrix. ~~To exclude the influence of actual temperature values, temperature deviation profiles, which are determined by subtracting the mean temperature of each profile from each level in the profile, are used as the SOM input in this study.~~ In addition~~The batch mode is chosen to execute the SOM algorithm.~~, the batch mode is chosen to execute the SOM algorithm~~This mode~~, because it is much more computationally efficient compared to the sequence mode. The other user-defined settings in the SOM software are set at the default, such as the hexagon topology, Gaussian neighborhood function, etc. The SOM code used in this study is sourced from the MATLAB SOM Toolbox, which is freely available from http://www.cis.hut.fi/projects/somtoolbox/.

2.3 Measuring the discriminative power of SOM technique for pollution assessment

The Kruskal-Wallis one-way analysis of variance is used as a non-parametric method to test the difference of pollutant concentrations among the various ABL types. A 1% significance level is used and hereafter denoted as *KW* in Sect. 3.2. Furthermore, the coefficients of variation (*CV*) of pollutant means across the various ABL types are also used to examine the discriminative power of the SOM technique for pollution assessment.

3 Results and discussion

3.1 Self-organized ~~ABL types~~boundary layer meteorology

We construct~~ed~~ a 3 × 3 SOM matrix for daily virtual potential temperature~~temperature~~ deviation profiles, and the ~~SOM~~ self-organized output shown in Fig. ~~1~~ 1 represents nine ABL types (i.e., SOM nodes). ~~In Fig. 1, the SOM~~

~~nodes are plotted in red, and the individual profiles corresponding to the SOM node are plotted in blue. For comparison, the mean and 25th and 75th percentiles for the entire period are plotted in cyan. On the SOM plane, the most notable feat~~On the SOM plane~~her~~ , the most notable feature is adjacency of like types (e.g., ~~nodes~~ Nodes 1 and 2) and the separation of contrasting types (e.g., ~~nodes~~ Nodes 1 and 9). ~~Although the SOM nodes appear to be sorted in a certain order, there is no physical significance associated with this order.~~ Such ordering is a feat~~her~~ure of the SOM algorithm (i.e., 'self-organized') ~~(i.e., 'self-organized'). This~~, which ~~feather~~ allows us to ~~visualize subtle differences between the neighboring clusters of profiles and~~ distinguish the unique characteristics of nodes through the variation of specific features across the SOM plane. According to the ordering feature, the SOM nodes in the four corners (i.e., Nodes 1, 3, 7 and 9) can be thought of as the typical types and the others can be considered as transitional types. The four typical ABL types have a relatively higher occurrence frequency (> 10%), with the highest frequency associated to Node 1 (23%). Furthermore, the seasonal statistical results (Fig. 2) reveal that these self-organized ABL types exhibit a strong seasonality. For example, Node 3 occurs more frequently in winter and autumn, while Node 1 has a relatively higher occurrence in spring and summer.

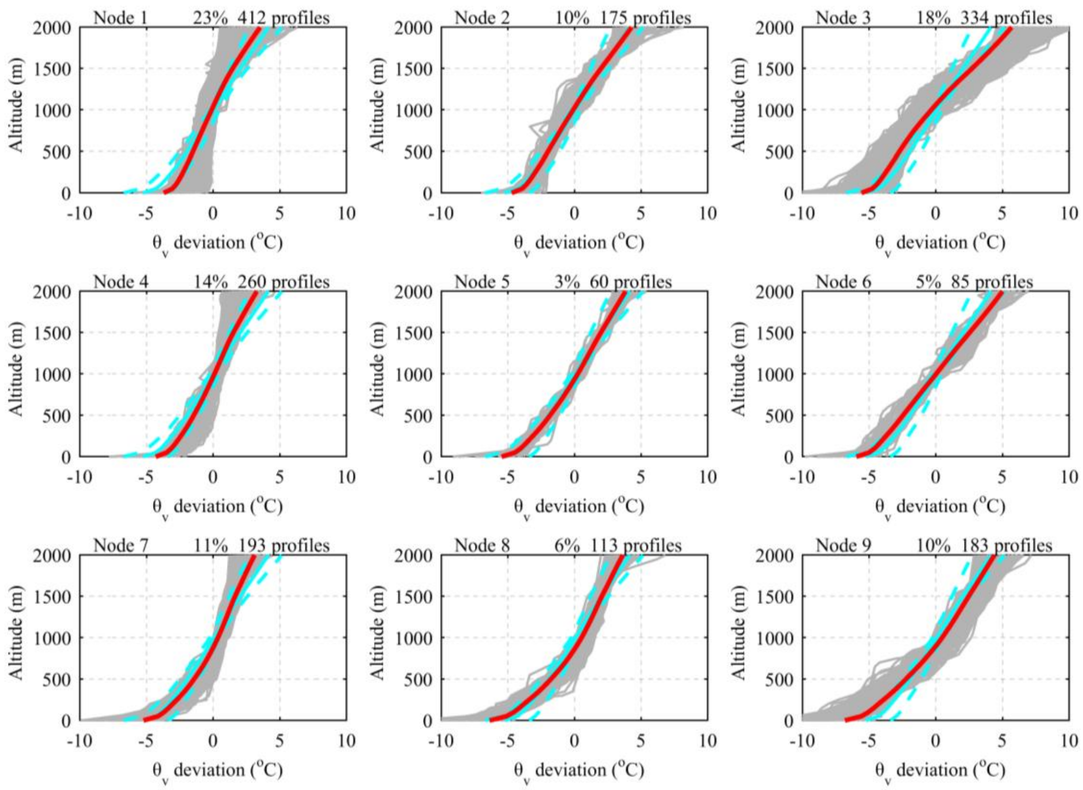

Figure 1. The 3 × 3 SOM output for radiosonde-based virtual potential temperature (θ_v~~T~~) deviation profiles observed at the Beijing Observatory. SOM nodes are shown in red, with the corresponding individual profiles in ~~dark blue~~grey. For reference, the overall average θ_v~~temperature~~ deviation profile and 25th and

75th percentile profiles are shown in cyan. The top-right shows the occurrence cases and frequency of each SOM node.

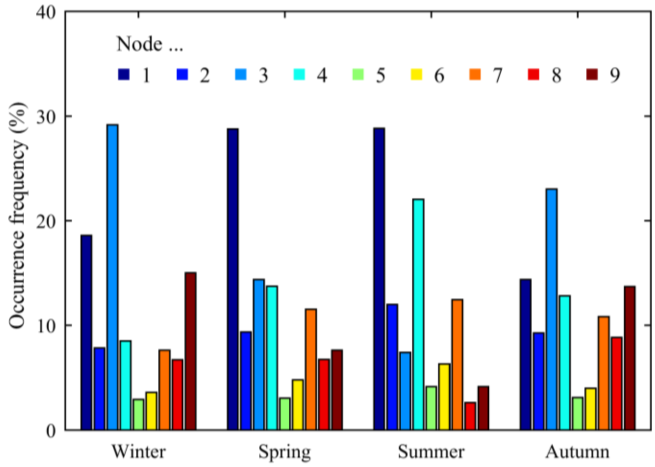

Figure 2. ~~Seasonality of SOM nodes shown as the relative frequency of seasons within each SOM node~~Relative frequency of individual ABL types (i.e., SOM nodes) in all four seasons. Winter (DJF); Spring (MAM); Summer (JJA); Autumn (SON).

~~The SOM classification reveals that for the whole study period, the ABL is dominated by near neutral to strong stable conditions, as none of the SOM nodes fall within the unstable category (i.e., super-adiabatic condition). The results are reasonable, considering the daily temperature profile is composited from 20:00 and 08:00 measurements. According to the SOM ordering feather, the SOM nodes in four corners (i.e., nodes 1, 3, 7 and 9) can be thought of as the typical ABL types and the others can be considered transitional ABL types. It is clear from the individual profiles in Fig. 1 that node 1 represents the well-mixed (near-neutral) condition with no temperature inversion, node 3 indicates the ABL type dominated by elevated inversion, node 7 indicates the ABL type dominated by surface inversion, and node 9 represents the ABL type associated with multiple inversions (i.e., including surface and elevated inversions).~~

~~Frequency analysis of the nine ABL types indicates that the frequency distribution across the types is quite varied from the expected 11.1 %, with the occurrence frequency showing a 5:1 range from the most frequent type (node 1) to the least frequent type (node 5). The higher-frequency types are presented on the outer portions of the SOM plane, while lesser-frequency types are presented closer towards the center (top-right in Fig. 1). The most dominant types are nodes 1 and 3, and their occurrence frequencies reach 22 % and 20 %, respectively. As~~

~~synoptic circulations change with the seasons over Beijing, the ABL types are expected to correspond to seasonality. The number of profiles from each season in each ABL type is expressed as a percentage and is shown in Fig. 2. All of the types exhibit strong seasonality. For example, node 1 has the highest occurrence in spring (29.4 %) and the lowest occurrence in autumn (13.7 %); node 9 presents the highest occurrence in winter (16.3 %) and the lowest occurrence in summer (4.9 %).~~

~~3.2 Evaluation against meteorological data~~

Figure 3 displays the average profiles of wind speed, relative humidity, virtual potential temperature gradient according to the ABL types~~Fig. 3 shows the average vertical profiles of potential temperature, wind speed and relative humidity corresponding to each ABL type~~. ~~As seen in Fig. ~~Clearly~~3~~, each of~~ the~~ the self-organized ~~ABL~~ types ~~is associated with~~features distinct dynamic and thermodynamic conditions within the ABL, suggesting the SOM technique is feasible to classify the boundary layer meteorology~~s~~. Since the classification is based on the twice-daily radiosondes, the resulting ABL types are dominated by near neutral to strong stable conditions, and none of the types fall within the unstable category (i.e., $\Delta\theta_v/\Delta z < 0$). While Node 3 features the strong static stability in the upper ABL (the large $\Delta\theta_v/\Delta z$ values), Node 1 represents a near neutral ABL condition with the lowest $\Delta\theta_v/\Delta z$ values and the highest wind shears in the lower ABL. In contrast, Node 7 corresponds to a moderate static stability in the lower ABL, and Node 9 relates to a strong static stability. Particularly, the virtual potential temperature gradient in Node 9 remains a high level (> 0.7^{o}C/100m) from surface to approximately 800 m, indicating a strong and deep surface temperature inversion developed in this type. In addition, due to the strong surface inversion, vertical mixing is suppressed, resulting in a strong decreasing gradient in humidity profiles. Overall, the SOM classification scheme reveals a significant coupling between dynamic and thermal effects in the ABL, which is expected to considerably impact the near-surface air quality.~~ The potential temperature profiles vary from near neutral conditions to strong stable conditions, and this change is closely related to the variance in wind speed, suggesting a strong coupling between the dynamic and thermal effects. The two extreme types (nodes 1 and 9) provide a very useful example. Node 9 is a very strong stable profile, and the wind speeds are very low in the lower ABL. In contrast, node 1 is a well-mixed (near neutral) profile and it corresponds to significantly higher wind speeds throughout the ABL. In addition, when the stability of the atmosphere is strong, vertical mixing is suppressed and winds in the lower ABL become decoupled from the generally stronger wind aloft. This allows moisture, fogs, low clouds and other scalars to build up within the stable layer. As a result, the stable ABL types usually correspond to high RH in the lower ABL.~~

~~The near-surface meteorological variables are also examined for each of the ABL types. Fig. 4 shows the diurnal composite plots of surface temperature, wind speed and relative humidity in the four typical ABL types. As expected, these near-surface variables respond well to the changing ABL structure. Wind speeds are the highest on the days corresponding to near neutral conditions (i.e., node 1). High wind speeds result in a deep, mechanically mixed layer, and these days also exhibited the smallest diurnal amplitude in wind speed, temperature and relative humidity. Such characteristics are likely consistent with the passage of frontal systems. In contrast, the smallest wind speeds are observed on days related to strong stable conditions (i.e., node 9). The stable days also generally exhibit the greatest amplitude of the diurnal signals in temperature and relative humidity. This fact is an indication that stable conditions occur mostly on clear sky days.~~

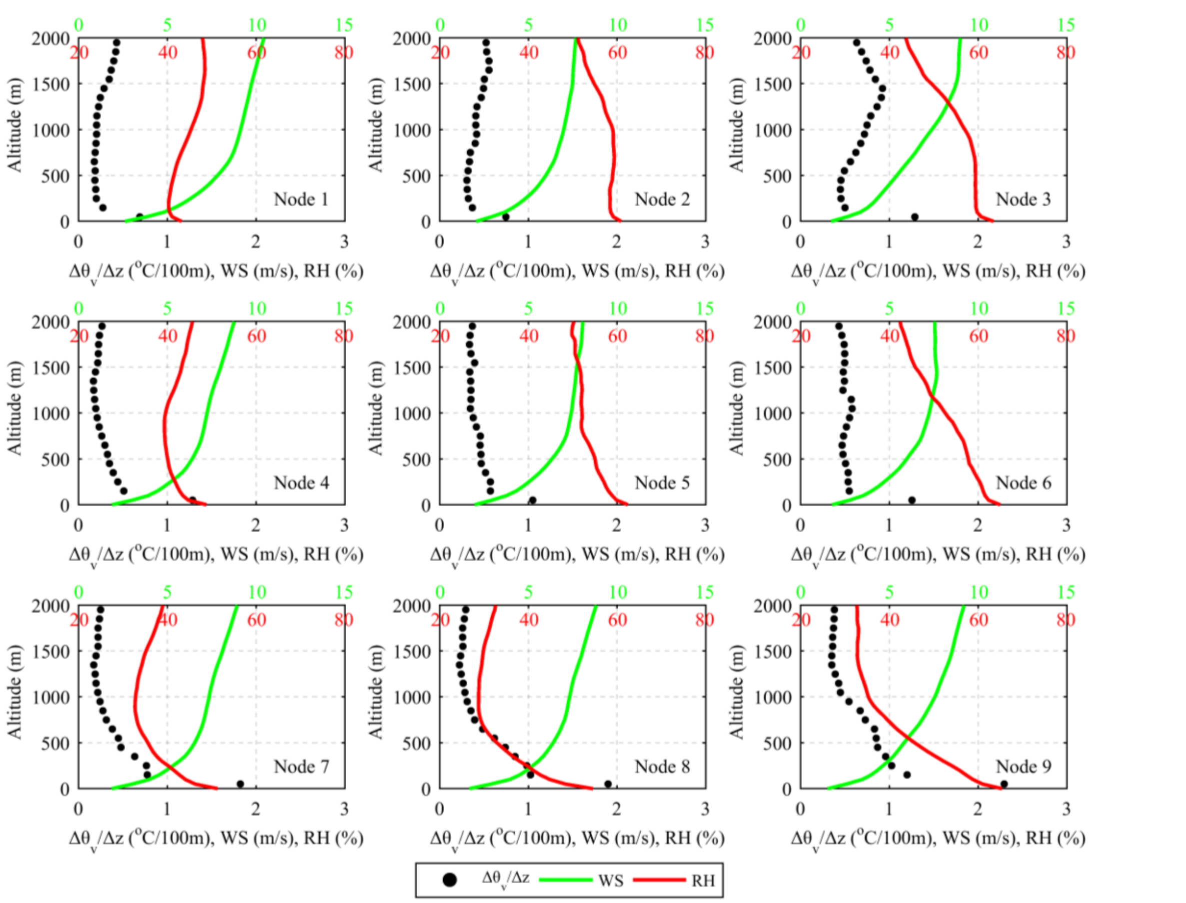

Figure 3. Profiles of average ~~potential temperature (θ),~~ wind speed (WS) ~~and~~, relative humidity (RH) and virtual potential temperature gradient ($\Delta\theta_v/\Delta z$) corresponding to individual ABL types (i.e., SOM nodes)~~each SOM node~~ at the Beijing Observatory. The black, green and red~~, green and black~~ labels of the horizontal axis correspond to $\Delta\theta_v/\Delta z$ ~~θ~~, WS and RH, respectively.

To detect the boundary layer development after sunrise, daytime boundary layer height (BLH) is estimated with parcel method (Holzworth, 1964, 1967), i.e., intersecting each day's 08:00 radiosonde potential temperature (θ) profile at Beijing Observatory with each hour's (from 09:00 to 15:00) surface θ values, which are calculated from surface air temperature observations. As shown in Fig. 4, the BLH on the days following a strong stable night (i.e., Node 1) is relatively flat, reflecting an inadequate development of daytime boundary layer. Similarity, Node 3 is also followed by a flat daytime BLH variation. The maximum BLH in these two types are lower than 900 m, indicating a limited space for vertical mixing in the day. In contrast, the afternoon BLH in Node 7 can reach up to 1100 m; this mixing depth is conducive to dilute the pollutants accumulated in the previous night. In Node 1, the convective boundary layer develops well, and its maximum height on average exceeds 1500 m, far higher than the values in other types.

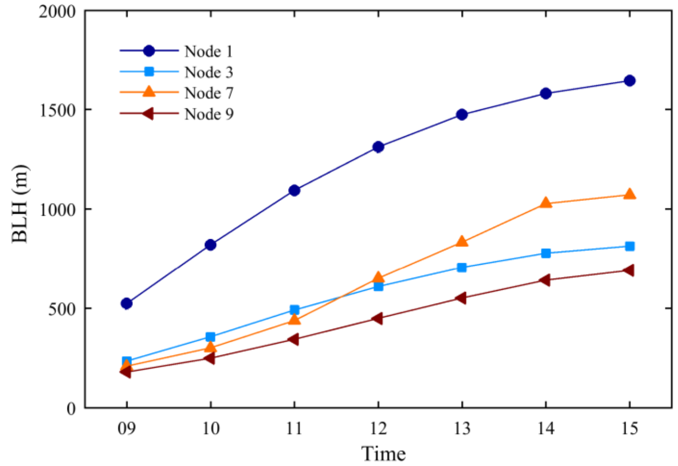

Figure 4. Daytime boundary layer height (BLH) estimated for the four typical ABL types (i.e., Nodes 1, 3, 7 and 9).

~~3.3 Evaluation against surface air quality~~

3.2 Implementing the SOM-based ABL classification scheme for urban air quality assessment

In the previous section, it was seen that the SOM classification scheme is an effective tool for delineation between various dynamic and thermodynamic structures within the ABL. As a further evaluation, we implement the new classification scheme to quantify changes in various urban pollutant concentrations as a function of ABL types. Since the pollutant emissions have a strong seasonality over Beijing and its surroundings, the analyses are performed for winter (December to February), spring (March to May), summer (June to August), and autumn (September to November), respectively. Figure 5 shows the statistical distributions of daily pollutant concentrations according to the nine ABL types, along with the results of Kruskal-Wallis test and the coefficients of variation of pollutant means across the various types. Figure 6 displays the type-average pollutant diurnal patterns composited for the four typical ABL types (i.e., Nodes 1, 3, 7 and 9).

~~The concentrations of gaseous and particulate pollutants in the atmosphere are governed by the rate at which they are emitted from their respective sources, lost by various sink mechanisms, and characteristics of the atmospheric volume into which they mix. While the mixing volume is determined primarily by the boundary layer structure, the chemical transformation also depends on boundary layer meteorology in some cases. In the previous section, it was seen that the SOM technique is an effective tool for classifying boundary layer structures. In this section, we used the classification technique to quantify the influence of the boundary layer structure on near-surface air quality.~~

~~Fig. 5 examines the daily concentrations of gaseous and particulate pollutants in relation to various ABL types.~~ The Kruskal-Wallis test demonstrates that the self-organized ABL types are able to distinguish between high and low loadings of air pollutants, with *KW* < 1% in all seasons (except for summertime SO_2 with a *KW* value of 1.5%). Furthermore, it is found that the SOM technique has a stronger discriminative power for SO_2, $PM_{2.5}$ and CO assessments, which is supported by relatively higher *CV* values (*CV*>0.30). According to the seasonal *CV* values, this discriminative power shows a following seasonal ordering: winter > autumn > spring > summer. Particularly, the wintertime *CV* value in $PM_{2.5}$ assessment reaches the maxima (0.56), indicating an extremely strong dependence of $PM_{2.5}$ air quality on the changing ABL meteorology in winter. In summer, the stable nocturnal ABL develops later due to the longer day (Li et al., 2012), and hence avoids the larger daytime pollutant emissions, particularly the traffic peak emissions. In the absence of larger sources, the nocturnal stable layers exert a limited influence on near-surface air quality; therefore, the classified ABL types have relatively weakened discriminative power for summertime pollution assessments. In addition, wet depositions (more precipitation in summer) play an important role in modulating summertime air quality, and to some degree disrupt the linkages between ABL type and air quality.

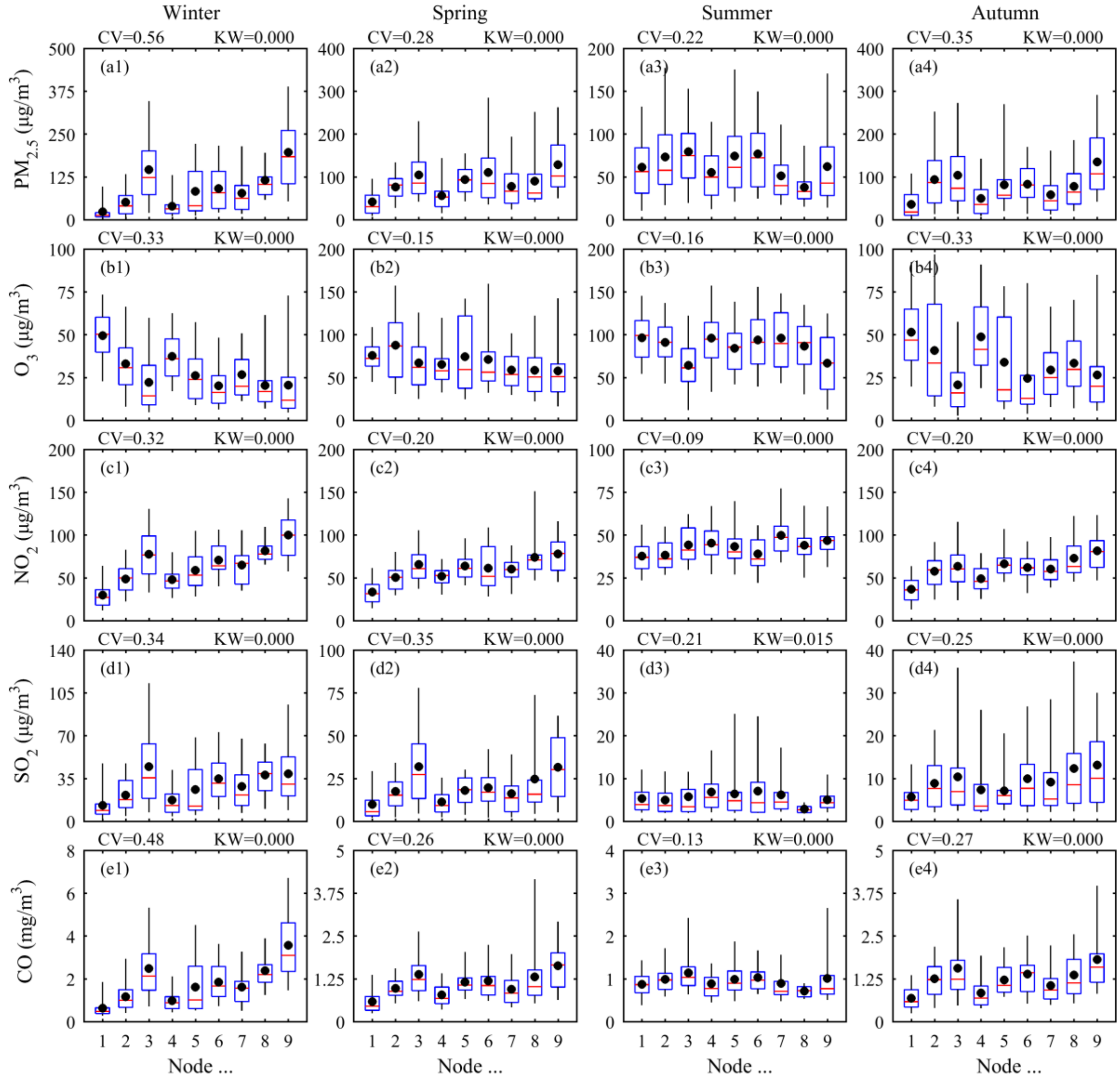

Figure 5. Daily concentrations of (a) $PM_{2.5}$, (b) O_3, (c) NO_2, (d) SO_2, and (e) CO in Beijing for all nine ABL types separately in (1) winter, (2) spring, (3) summer, and (4) autumn. The solid dots denote the mean. The box and whisker plot presents the median, the first and third quartiles, and the 5th and 95th percentiles, respectively. The upper numbers denote the results of Kruskal-Wallis test (*KW*) and the coefficients of variation (*CV*) of pollutant means across the various types.

In the case of $PM_{2.5}$, NO_2 and CO, the most stable atmospheric conditions (i.e., Node 9) are associated with dramatically increased near-surface pollutant concentrations in all seasons except summer. The wintertime average concentrations of $PM_{2.5}$, NO_2 and CO in Node 9 reach up to 197.2 μg/m^3, 100.2 μg/m^3 and 3.6 mg/m^3, respectively. These values are 3–8 times higher than that in Node 1 (i.e., near neutral condition), with the highest increasing amplitude (a factor of 7.3) related to $PM_{2.5}$. As have known, Node 9 corresponds to the strongest nighttime stability in the lower ABL and the lowest daytime BLH. All of these ABL characteristics are extremely conducive to the accumulation of air pollutants emitted near the ground. For Node 3, the concentrations of $PM_{2.5}$, NO_2 and CO are the second-highest compared to those of the other types. This ABL type features the strongest stability in the upper ABL, suggesting that processes operating at the different heights throughout the ABL may have a significant impact on near-surface pollutant concentrations.

The diurnal cycles of $PM_{2.5}$, NO_2 and CO are extremely pronounced under the strong stable conditions, although very reduced on the days with near neutral night. On average, the wintertime diurnal range of $PM_{2.5}$ increases from 18.2 μg/m^3 in Node 1 to 95.4 μg/m^3 in Node 9. The corresponding diurnal range increase for NO_2 is 18.9 to 33.6 μg/m^3, and for CO 0.2 to 1.7 mg/m^3. In Node 1, the diurnal variations are characterized by a weak two-peak pattern following the traffic rush hours, suggesting that traffic is the primary driver of these pollutants' diurnal cycles in Beijing (Liu et al., 2012). However, the diurnal effects of traffic emissions are significantly amplified by the ABL dynamics. It is clear that the more stable conditions near the ground, the higher peak concentrations are observed. In winter, the stable ABL conditions exert a more important influence on the evening traffic emissions, resulting in a broad evening peak. In contrast, the morning peak signature is much lower since the morning emission is counteracted by the destabilization of the ABL. However, as human activities begin earlier during the warm season, maximum concentrations in spring and summer are typically observed during the morning rush hours.~~(Pernigotti et al., 2007;Chambers et al., 2015b;Crawford et al., 2016;Chambers et al., 2015a)~~

However, increasing atmospheric stability has the opposite effect on near-surface O_3 concentrations. Since aerosols can absorb and reflect solar radiation and thereby inhibit the photochemical production of O_3 (Gao et al., 2016;Kaufman et al., 2002), the lowest average O_3 concentration is observed in Node 9. In addition, considering that ozone is mainly produced in the upper ABL, near-surface O_3 should be strongly modulated by down-mixing processes (Tang et al., 2017b;Tang et al., 2017a). In this light, the varying daytime O_3 peaks across the ABL types can be partly attributed to the various magnitudes of vertical mixing. This is supported by daytime BLH. As have shown in Fig. 4, the daytime BLH is highest in Node 1, followed by Node 7, Node 3 and the lowest in Node 9. Such ordering is generally consistent with the daytime O_3 peaks in these types. Due to the persistent down-mixing caused by strong wind shears, the near-surface O_3 remains a relatively high nocturnal concentration (e.g. about 45 μg/m^3 in winter) in Node 1. In contrast, the stable nocturnal conditions (e.g., Nodes 9, 7 and 3) are commonly associated with low O_3 concentration (e.g. about 16 μg/m^3 in winter) due to the lack of vertical mixing, as well as the strong chemical titration by NO emitted from vehicles.

~~As expected, the most stable conditions are associated with a dramatic increase in the mass concentrations of air~~

~~pollutants (except O_3). On average, SO_2, NO_2, CO, PM_{10} and $PM_{2.5}$ increase by 15.7 μg/m^3 (142 %), 44.3 μg/m^3 (119 %), 1.5 mg/m^3 (202 %), 91.6 μg/m^3 (119 %) and 95.9 μg/m^3 (218 %) from the near neutral ABL condition (i.e., node 1) to strong stable condition (i.e., node 9), respectively. The highest increasing amplitude is related to $PM_{2.5}$, suggesting fine particulate matters are likely accumulated from not only primary emissions but also secondary formation (Zhang and Cao, 2015). As we have shown, the more stable ABL conditions tend to correspond to high relative humidity in the lower ABL (Figs. 3 and 4). Additional enhancement in $PM_{2.5}$ can be expected under the humid condition, as it is known that the humidity-related physicochemical formation of particles (such as hygroscopic growth, liquid-phase and heterogeneous reactions) can be intensified by high humidity values (Cheng et al., 2015;Cheng et al., 2016;Zheng et al., 2015).~~

~~Interestingly, increasing atmospheric stability has an opposite effect on near-surface O_3 concentrations. Since O_3 is produced by photochemical interactions between NO_x (NO + NO_2) and volatile organic compounds (VOCs) (Seinfeld and Pandis, 2006), the boundary layer structure alters the O_3 level through modulation of its precursors (NO_x and VOCs). The low O_3 level in the stable ABL can be explained by the strong titration reaction. Since O_3 is highly reactive, when trapped in a stable layer, surface titration by the NO emitted from vehicles can cause a rapid reduction in O_3 concentration. In previous studies, persistent low O_3 concentration were observed in the stable boundary layer condition in Beijing (Zhao et al., 2013). Conversely, when near-surface wind speeds are higher (near neutral condition such as node 1), O_3 is mixed downward from the overlying air mass, resulting in higher concentrations. Nevertheless, it is worth noting that the extremely high O_3 values (not shown) were also detected on very stable days (i.e., node 9), suggesting the complexity of O_3 behavior in response to the boundary layer structure (Tong et al., 2011;Haman et al., 2014).~~

~~To obtain a more in-depth understanding of the physical mechanisms behind the relationship between air quality and ABL structure, diurnal composite hourly concentrations of atmospheric pollutants are formed for each ABL type.~~

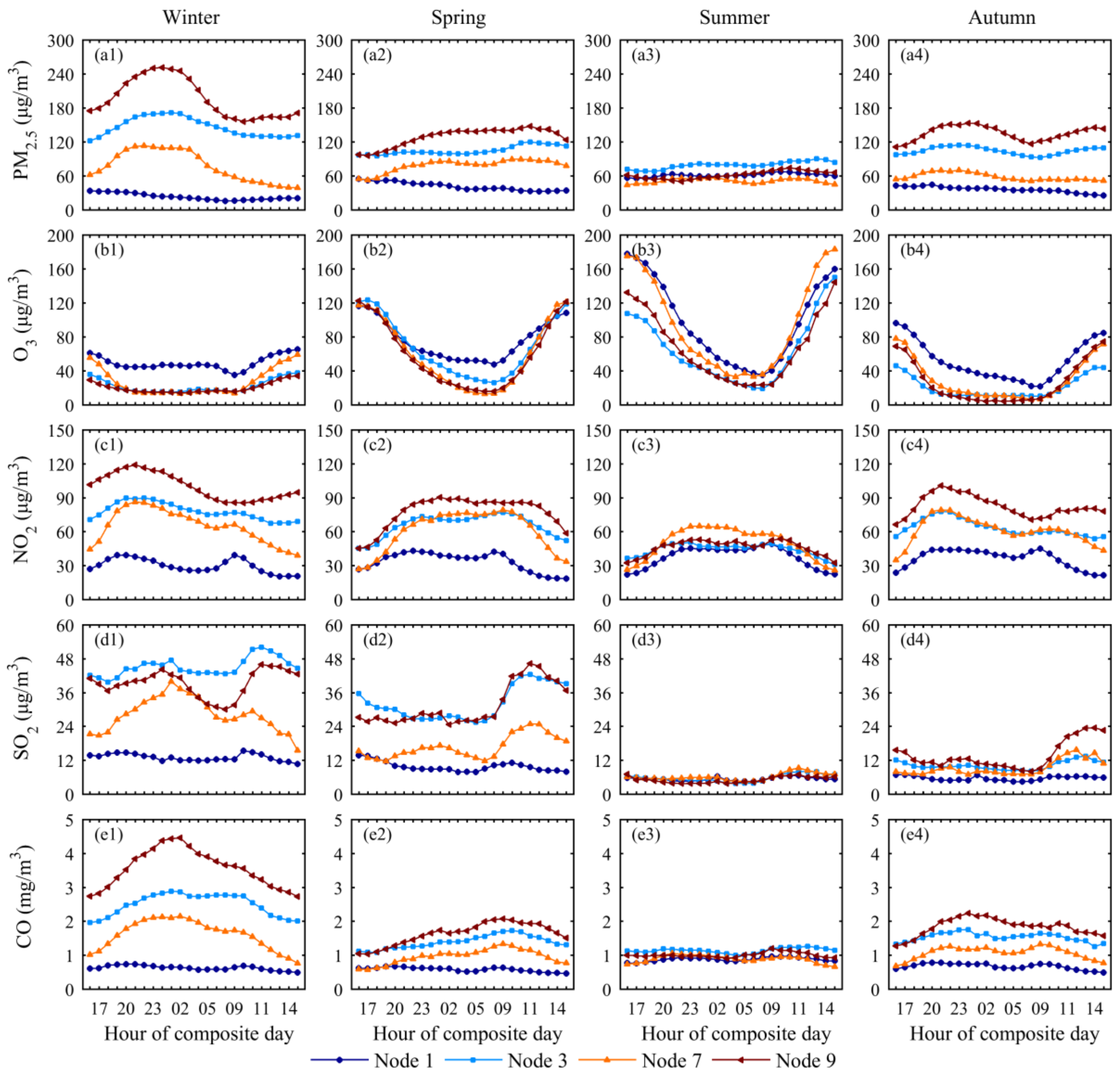

Figure 6. Mean hourly composites of (a) $PM_{2.5}$, (b) O_3, (c) NO_2, (d) SO_2, and (e) CO in Beijing for the four typical ABL types separately in (1) winter, (2) spring, (3) summer, and (4) autumn

~~The SOM-based ABL classification scheme provides a consistent, gradual distinction in the diurnal cycles of surface air pollutants from near neutral to strong stable conditions. The composite diurnal evolutions of air pollutants in the four typical ABL types (i.e., nodes 1, 3, 7 and 9) are illustrated in Fig. 6. (Tang et al., 2017b;Tang et al., 2017a)~~

The highest average SO_2 concentrations are typically observed in Node 3, but occasionally in Node 9. Over the North China Plain, high stacks are emitting a significantly larger amount of SO_2 compared to small stacks (Zhao et al., 2012). The frequent surface temperature inversions together with the large SO_2 emissions from higher stacks favor the formation of elevated SO_2 pollution layers over Beijing (Chen et al., 2009). If sufficiently strong, the surface temperature inversion can even isolate near-surface observations from the influence of elevated pollution layers (Salmond and McKendry, 2005). This explains the commonly lower near-surface SO_2 concentration in

Node 9 than that in Node 3. However, after a stable night, the burst of turbulent activity in the morning coincides with a rapid increase in near-surface SO_2 concentration, resulting in a pre-noon peak. Since there is no significant increase in SO_2 emission at the surface at that time, the result strongly suggests that the SO_2 peaks are due to the downward mixing from the elevated SO_2 pollution layers. Regarding the physical mechanism of the noontime-peak SO_2 pattern, Xu et al. (2014) have made a detail explanation in a previous study. Nevertheless, the wintertime SO_2 concentration signature does not always show a distinct pre-noon peak (e.g., Node 7). This may attribute to the increased SO_2 emissions from household heating in winter (Liao et al., 2017). Like other primary pollutants, the local SO_2 emissions become trapped close to the surface under the stable nocturnal condition, resulting in a much higher nighttime peak compared to the pre-noon peak.

~~The diurnal cycles of SO_2, NO_2, CO, PM_{10} and $PM_{2.5}$ are extremely pronounced under the strong stable condition (i.e., node 9), although very reduced under the near neutral condition (i.e., node 1). In contrast, the behavior of O_3 is completely different from other pollutants. The results suggest that the chemical species, which are mainly produced by surface emissions, are strongly modulated by the development of the ABL, while the chemical species, which are strongly controlled by the photochemical process, are weakly regulated by the development of the ABL (Crawford et al., 2016). Overall, the diurnal behavior of each pollutant species in each of the ABL types is generally consistent with the existing knowledge for urban areas (Chambers et al., 2015b;Chambers et al., 2015a;Zhang et al., 2012b;Jenner and Abiodun, 2013;Han et al., 2009).~~

~~Of particular interest in Fig. 6 is that (1) nodes 3 and 9 have similar magnitudes of concentrations in the afternoon, and (2) nodes 7 and 9 have similar increments in concentrations from afternoon to midnight, although there is a huge distinction in the afternoon concentrations (i.e., afternoon baselines). This sheds some light on the common patterns of the ABL controls on the near-surface air quality in Beijing. Considering the thermal inversion feather in each of ABL types (Fig. 1), the regulating effects of ABL on near-surface concentrations can be concluded as follows: (1) elevated inversion enhances the afternoon baseline; and (2) surface inversion improves the evening increment. Obviously, the high afternoon baselines in nodes 3 and 9 can be attributed to elevated inversion, while high evening increments in nodes 7 and 9 can be attributed to surface inversion. Since surface inversion usually develops shortly before sunset due to radiation cooling, the evening traffic emission peak is counteracted by a stabilizing boundary layer. Consequently, the air pollutants such as NO_2, CO, PM_{10} and $PM_{2.5}$ often experience an explosive growth from afternoon to midnight. In contrast, elevated inversion usually forms due to synoptic forcing (such as synoptic advection) (Hu et al., 2014;Xu et al., 2016) and can persist for several days; as a result, the daytime mixing volume is also depressed, causing a relatively higher afternoon~~

~~concentration.~~

~~Beijing has relatively little industry but numerous automobiles, and the emissions of SO_2 are small while those of CO, NO_x and particles are much larger (Zhao et al., 2012). By comparison, the diurnal behaviors of SO_2 and other pollutants are completely different. For example, in node 9, SO_2 show a lower nighttime concentration but a sharp increase after sunrise, whereas NO_2, PM_{10} and $PM_{2.5}$ show a higher nighttime concentration with a slight morning increase associated with the traffic emission. The results largely suggest that the changing ABL structure affects the near-surface observations of locally and remotely sourced pollutants in very different ways. In the evening, since the stable boundary layer (SBL) and the residual layer (RL) are essentially decoupled with each other (Stull, 1988), locally sourced pollutants emitted into the surface layer (such as CO, NO_2 and particulate matters from vehicular emissions) become trapped close to the surface. In contrast, remotely sourced pollutants emitted from chimneystacks above the SBL (such as SO_2 from power plants in the Hebei Province) may be stored within the RL aloft and not penetrate into the SBL. As the daytime convective turbulent mixing developed in the morning, the rapid momentum transfer between the surface and aloft air transported the pollutants stored in RL downward and meanwhile upwardly mixed the pollutants trapped from the previous night in the surface layer (Salmond and McKendry, 2005). It is observed in Fig. 6 that after a stable night, the burst of turbulent activity in the morning coincides with a rapid increase in SO_2 concentration (Fig. 6). Since there is no significant increase in SO_2 emission at the surface at this time, this result strongly suggests that increased SO_2 in the morning resulted from the downward mixing of stored SO_2 in the RL aloft. In a previous case study, Li et al. (2017) reported that as a result of both turbulent mixing and the advection of high concentrations of air pollutants above the surface layer, the urban area of Beijing experienced a dramatic increase of the $PM_{2.5}$ concentration in the morning on 30 November 2015.~~

~~Given the importance of local vehicle emissions vs. more-distance power plant and industrial emissions for Beijing's air quality, the ratio of CO/SO_2 can be considered as an indicator of the contribution of local emissions to air pollution, with higher ratios indicating higher local contributions (Tang et al., 2015). Fig. 7 shows the composite diurnal variations of CO/SO_2 ratios in the four typical ABL types (i.e., nodes 1, 3, 7 and 9). The contrasts between CO/SO_2 ratios for the various ABL types are noticeable during the nighttime, whereas differences during the daytime are minimal. During the daytime, when the ABL is well mixed, near-surface pollutant concentrations represent a combination of local and remote sources. In the evening, however, the earth's surface begins to cool, and a stable boundary layer begins to form from the ground up. If sufficiently strong, the~~

~~nocturnal surface inversion can isolate near-surface observations from the influence of distant sources (Crawford et al., 2016). Consequently, the more stable the nocturnal conditions near the ground, the higher the CO/SO_2 ratios that occur (Fig. 7). The results are consistent with previous studies (Tang et al., 2015;Zhu et al., 2016), indicating local contribution increases with enhanced static stability in the surface layer over Beijing. According to the above analysis, high pollutant loadings in node 9 are mostly attributable to local contributions (the highest CO/SO_2 ratios in node 9); however, high pollutant loadings in node 3 are more likely due to regional contributions (the lowest CO/SO_2 ratios in node 3). Obviously, it is the stable stratification rather than the weak surface wind that confines the regional contribution.~~

~~3.4 Evaluation against columnar aerosol pollution~~

~~For many years, aerosol particles have been the primary pollution problem in Beijing. Atmospheric aerosols play an important role in radiation transfer due to absorption and/or scattering in the atmosphere, and thus could have a great influence on the evolution of the ABL. In recent years, the feedback effect of aerosols on the ABL has drawn much attention . To further our understanding of aerosol pollution in Beijing, we examine the optical and physical properties and the direct radiative forcing of columnar aerosols in the different ABL types in this section.~~

~~Aerosol optical properties can be characterized by three useful parameters: AOD, AE and SSA. Fig. 8 illustrates the AOD_{440nm}, $AE_{440nm\text{-}870nm}$ and SSA_{440nm} over Beijing within the nine ABL types. The ABL-type averages of AOD range from 0.52 and 1.22 (Fig. 8a). Comparing with near-surface observations, the greatest difference is that the highest AOD value generally occurs in node 3, rather than in node 9 (the highest surface $PM_{2.5}$ and PM_{10} concentrations occur in node 9). This may be attributed to the difference in aerosol vertical distribution in these two types. As we have demonstrated in Sect 3.3, node 3 is related to strong regional transport. Since the height of regional transport is usually above the surface layer, such as 200–700 m AGL detected by , more aerosol particles might be suspended above the surface layer in node 3, resulting in the highest AOD value in the atmospheric column. In addition, since high relative humidity also occurs in node 3, the highest AOD value in this ABL type could be partly attributed to the particle hygroscopic growth.~~

~~It is known that high AE values indicate a dominance of fine particles, while low values indicate a dominance of coarse particles. Unlike AOD, the AE shows a relatively low sensitivity to ABL types (Fig. 8b). All type averages of AE are higher than 1.0, suggesting that the proportion of fine particles is always larger than that of coarse particles over Beijing . The highest AE occurs in node 6 (1.20) and the lowest is 1.03 in node 1. Node 1~~

~~corresponds to the lowest AE value, indicating that under the near neutral ABL condition, the coarse particles contribute a relatively higher proportion of total particles. This could be due to the increasing wind speed with decreasing relative humidity (Figs. 3 and 4). Coarse particles could be from more natural and anthropogenic dust emission under high wind speed conditions. Particularly during the fast northwesterly wind period, dust storms occasionally contribute to the high coarse particle loadings in Beijing . The long-distance transport of dust particles from northwest China may be the reason for the lowest AE value in node 1.~~

~~The SSA is defined as the ratio of the scattering coefficient and the total extinction coefficient. It is mostly dependent on the aerosol size, concentration of absorbing component and its mixture state with non-absorbing components. The daily SSA at 440 nm ranges from 0.82 to 0.98 during the study period, which suggests that there are quite different types of aerosols in the columnar atmosphere over Beijing (varying from strong absorbing aerosols to strong scattering aerosols). It is easy to see that the ABL types associated with a strong surface inversion (i.e., nodes 7, 8 and 9) have lower SSA values (Fig. 8c). The averaged SSA in these nodes is approximately 0.90, which is significantly lower than that in nodes 1, 2 and 3. The low SSA values mean enhancement in the absorbing particles, such as black carbon, which are released from industry, biomass/biofuel burning, diesel vehicle, and coal burning. In contrast, the highest SSA occurring in node 1 can be explained by dust particle transmission and soil aerosol emissions.~~

~~The volume particle size distribution retrieved in the sizes between 0.05 and 15 μm is one of the most important parameters for studying the behavior of aerosols . Fig. 9 expresses the mean volume particle size distribution (dV/dln$R$) over Beijing in the nine ABL types. Table 1 supplements Fig. 9 with the statistical parameters of aerosol particle size distribution. Clearly, the volume particle size agrees very well with the bimodal lognormal distributions. Both fine (R < 0.6 μm) and coarse (R > 0.6 μm) modes exhibit relative stability with two peaks at a radius of approximately 0.1–0.2 μm and 2.0–4.0 μm, which are similar to some previous studies. However, the size distribution shows a distinct difference in the changing amplitude for different ABL types. The fine- and coarse-mode particle volumes increase rapidly from left (nodes 1, 4 and 7) to right (nodes 3, 6 and 9) on the SOM plane. This suggests that with the stabilizing boundary layer processes, the atmosphere is more loaded with both fine- and coarse-mode particles over Beijing. In addition, the stabilizing processes are accompanied by the increase of the fine-mode effective radius (R_{eff}-F) and fine-mode volume fraction (Vf/Vt). These results strongly point to the important role of fine-mode particle hygroscopic growth on the days associated with stable nocturnal ABL conditions.~~

~~The type-averaged ARF at the surface (BOA), top of atmosphere (TOA), and within the atmosphere (ATM) over Beijing is shown in Fig. 10. The type averages of ARF at the surface range from -47.8 W/m^2 to -110.0 W/m^2, while at the TOA, they are found to be between -21.1 W/m^2 and -48.0 W/m^2. Likewise, the ABL type averaged ARF within the atmosphere are between 26.7 W/m^2 and 63.1 W/m^2. The larger negative ARF at the surface (> 110 W/m^2) and positive ARF within the atmosphere (> 60 W/m^2) are found in ABL types 3, 6 and 9 over Beijing, implying strong cooling at the surface and warming in the atmosphere. These results are induced by relatively larger aerosol loadings under the stagnant meteorological conditions. The larger ARF within the atmosphere demonstrates that solar radiation is being absorbed within the atmosphere, and as a result, heats the atmosphere and reduces surface temperature. This can change the atmospheric vertical temperature gradient and improve the atmospheric stability. Finally, the enhanced stability hinders the vertical diffusion of aerosol particles, leading to the increase of aerosol concentrations and causing a further decrease in the solar radiation and ABL height, which induces a positive feedback loop for causing high surface aerosol concentrations .~~

~~3.5 Evaluation against heavy polluted episodes~~

3.3 Quantifying the contribution of ABL anomaly to typical-month $PM_{2.5}$ air quality

To improve air quality, the Chinese government promulgated "Air Pollution Prevention and Control Action Plan" in 2013. As a consequence, observed annual mean $PM_{2.5}$ concentrations decrease by about 37% over Beijing during 2013-2017. However, severe wintertime $PM_{2.5}$ pollution events still frequently wreaked havoc across Beijing and its surroundings, which resulted in severe damages to the environment and human health (Gao et al., 2017;Gao et al., 2015). It is therefore pressing to understand the factors affecting the occurrence of such serious $PM_{2.5}$ pollution. Previous studies highlighted potential importance of atmospheric conditions to the wintertime $PM_{2.5}$ air quality (Cai et al., 2017). Since the fraction of time for which the different atmospheric conditions dominate can vary from year to year, elucidation of the meteorological roles in those serious pollution periods has a significant importance. In this section, we evaluate the contribution of ABL anomaly to elevated $PM_{2.5}$ concentration in three typical pollution months, i.e., January of 2013, December of 2015 and December of 2016.

~~In 2013, the Chinese State Council released the "Atmospheric Pollution Prevention and Control Action Plan" to implement a megacity cluster-scale joint prevention and control strategy program. As a result, the $PM_{2.5}$ in Beijing decreased from 89.5 μg/m^3 in 2013 to 73.0 μg/m^3 in 2016. However, these meteorology-driven pollution episodes to some degree obscure the true impacts of the emission control strategies implemented by governmen t.~~

~~In January of 2013, December of 2015, and December of 2016, H~~heavy $PM_{2.5}$ ~~aerosol~~ pollution episodes occurred frequently in January of 2013, December of 2015 and December of 2016 ~~wreaked havoc across Beijing,~~ resulting in anomalously high month-averaged $PM_{2.5}$ concentrations in the Beijing urban area (180.1 μg/m^3, 151.8 μg/m^3 and 151.2 μg/m^3, respectively)~~and its surroundings, which resulted in severe damages to the environment and human health~~. Fig~~.~~ure ~~11~~ 7 shows the hourly $PM_{2.5}$ variations~~s of $PM_{2.5}$ and AOD_{440nm} during~~in the three ~~three heavily polluted~~selected months, along with daily ABL types. ~~It is observed that the $PM_{2.5}$ concentrations were frequently elevated to above 200 μg/m^3, and the AOD often exceeded 1.0 in Beijing~~ In general~~during these three months. The ABL types (shown at the top of each plot) reveal that~~, the pollution ~~episodes~~ episodes were ~~generally~~ associated with ~~the control of nodes~~ Nodes 3 and 9, and the clean ~~episodes~~ episodes ~~were often associated with~~corresponded to ~~the control of node~~ Node 1. For example, the severe pollution episode that occurred from 9–14 January 2013 was due to the alternate ~~control~~ control of ~~nodes~~ Nodes 3 and 9, and the pollution episode from 15–21 December 2016 was related to the persisten~~t control~~cy of ~~node~~ Node 9. ~~In contrast~~Conversely, multiday control of ~~node~~ Node 1 caused a clean episode from 14–16 December 2015. The linkages between $PM_{2.5}$ air quality and ~~the boundary layer structure~~ABL type ~~were~~ are consistent with the ~~long-term~~previous long-term analyses ~~described in Sects. 3.3 and 3.4~~, indicating that the changing ABL type~~types~~ is~~are~~ one of the primary drivers of day-to-day variations in wintertime $PM_{2.5}$ air quality over Beijing.

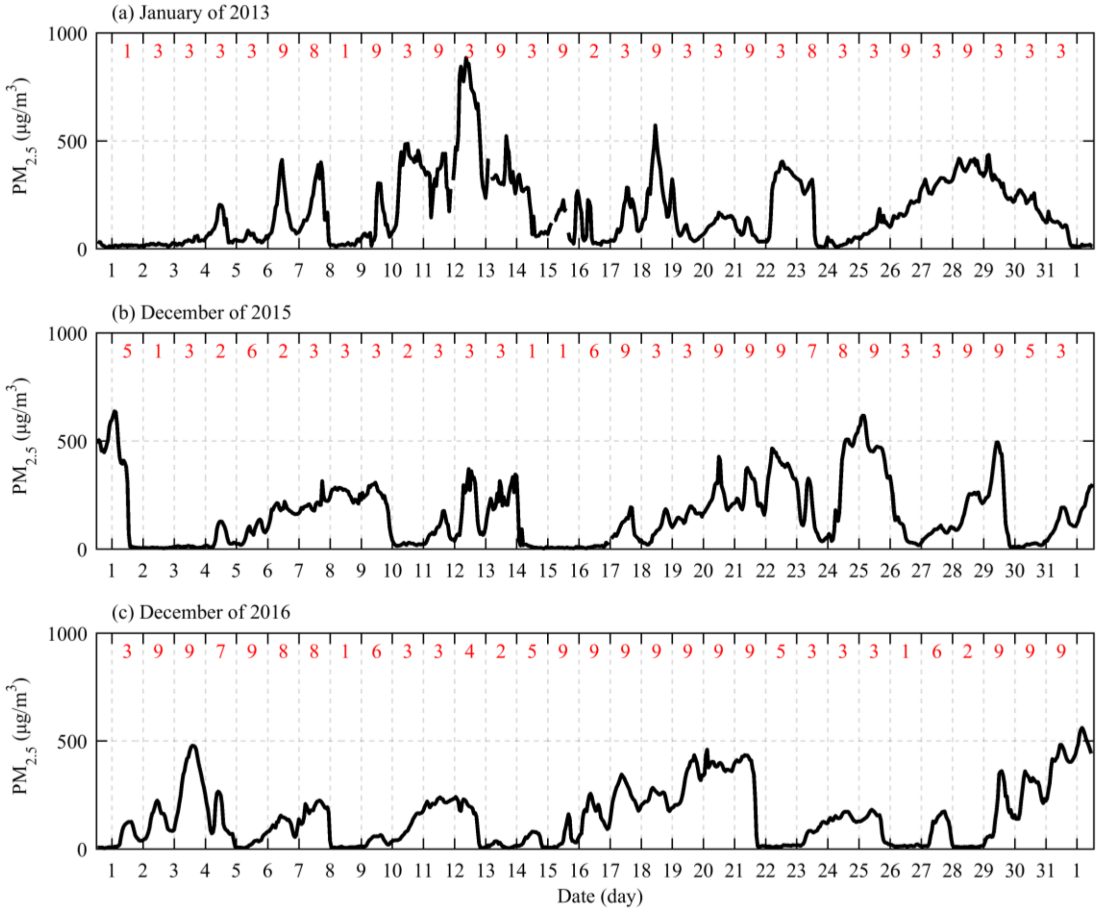

Figure 7. Time series of hourly $PM_{2.5}$ concentrations in (a) January of 2013, (b) December of 2015, and (c) December of 2016. The daily ABL types (i.e., SOM nodes) are shown at the top of each plot (red numbers).

~~The monthly $PM_{2.5}$ concentrations in the Beijing urban area reached up to 180.8 μg/m^3, 153.9 μg/m^3 and 147.9 μg/m^3 in January 2013, December 2015 and December 2016, respectively. All these values were far larger than the 4-yr winter mean $PM_{2.5}$ concentration (110.6 μg/m^3). Although the characteristics of $PM_{2.5}$ air quality depend on many complex elements, the major contributors are the pollutant emissions and meteorological conditions. In 2013, the Chinese State Council released the "Atmospheric Pollution Prevention and Control Action Plan" to implement a megacity cluster-scale joint prevention and control strategy program. As a result, the $PM_{2.5}$ in Beijing decreased from 89.5 μg/m^3 in 2013 to 73.0 μg/m^3 in 2016. However, these meteorology-driven pollution episodes to some degree obscure the true impacts of the emission control strategies implemented by government.~~ Fig~~.~~ure 8~~12~~ ~~shows~~ illustrates a comparison of the occurrence frequency of the nine ABL types between ~~to the winter mean frequency (2013-2016) for~~ the ~~three~~ three selected~~polluted~~ months and the whole 5-year winter period. Compared with the~~ 4-yr~~ winter~~ mean~~-averaged frequency, ~~the greatest~~ notable differences are that the ~~occurrences of nodes~~ stable ABL conditions~~3 and 9 (the two most polluted types)~~ increased and the ~~node~~ near neutral nights~~1 (the clean~~

~~type)~~ decreased during the three polluted months. For example, Node 9 occurrence was nearly trebled in December of 2016, and total occurrence of Nodes 3 and 9 doubled in January of 2013. These results highlighted potential contribution of ABL anomaly to the elevated $PM_{2.5}$ concentrations in these polluted months.~~Obviously, the elevated $PM_{2.5}$ concentrations in the abovementioned months can be mostly attributable to the anomalous boundary layer structures.~~

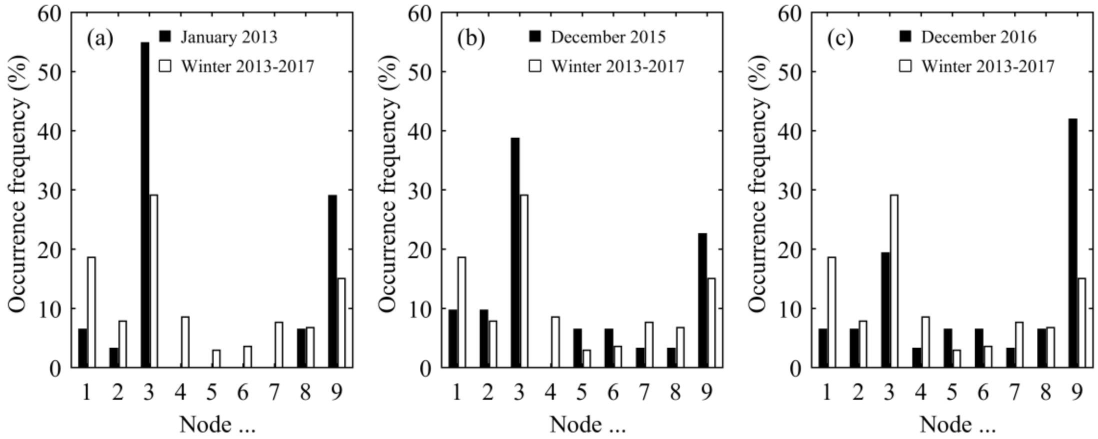

Figure 8. Occurrence frequency of the ABL types (i.e., SOM nodes) during (a) January 2013, (b) December 2015, and (c) December 2016. The winter-averaged frequency during the 5-year (2013–2017) period is repeated on each plot for comparison.

Assuming the linkages between ABL type and $PM_{2.5}$ loading are constant in different years, the contribution of the anomalous ABL meteorology to $PM_{2.5}$ air quality can be estimated through a meteorology-to-environment method, which is revised from the circulation-to-environment method proposed by Zhang et al. (2012). ~~Quantitative analysis of the roles of the ABL anomaly in $PM_{2.5}$ variations during the pollution months is helpful for the assessment of air pollution prevention and control strategies. In this study, the ABL classification allows for the integrated evaluation of the effects of numerous interrelated ABL meteorological parameters on air quality. Here, a meteorology-to-environment method (revised from the circulation-to-environment method proposed by Zhang et al. (2012a)) is utilized to evaluate the influence of the ABL anomaly for enhanced $PM_{2.5}$ levels during the abovementioned months. We a~~For each selected month~~ssume the linkages between ABL types and their $PM_{2.5}$ loadings in winter are constant in different years.~~ , we define ~~For each polluted month, the total anomaly (C') is defined as~~ the deviation in $PM_{2.5}$ from the ~~4~~5-year ~~winter~~ winter-averaged~~mean~~ concentration (C_{WIN} ~~$\overline{C}$~~) as the total anomaly (C')~~. This total anomaly~~, which ~~in each month~~ is due to the combined effects of emission and meteorology ~~and emission~~. The anomaly calculated from the mean $PM_{2.5}$ loadings for nine ABL types and their occurrence frequencies during each month can be considered as the "ABL-driven" anomaly, which~~to~~ represents the $PM_{2.5}$ change caused by the anomalous ~~boundary layer~~ABL ~~structure~~meteorology. ~~We refer to this as the "ABL-driven" anomaly.~~ The ABL-driven anomaly (C_{ABL}') is calculated through – $\sum_i F_i \cdot C_i - C_{WIN}$, where F_i is the occurrence frequency of type-*i* ABL during a specific month~~period~~ and C_i is the corresponding $PM_{2.5}$ loading ~~feather~~featuring that type. The ratio of C_{ABL}' to C' ~~(the difference of C_{ABL}' to $\bar{C}$)~~ is then used to ~~evaluate~~ assess the relative ~~(absolute)~~ contribution of the ABL anomaly to the total anomaly~~enhanced $PM_{2.5}$ level~~. The calculated results (Table 1) shows that the ABL-driven $PM_{2.5}$ changes are 44.4 μg/m^3 in January 2013, 22.2 μg/m^3 in December 2015, and 34.6 μg/m^3 in December 2016, which explain 58.3%, 46.4% and 73.3% of total anomaly in respective month. ~~The results show that the contributions of the frequency anomaly of the ABL type to the increase in $PM_{2.5}$ are 65.8 % (46.2 μg/m^3) during January 2013, 46.7 % (20.2 μg/m^3) during December 2015 and 94.6 % (35.3 μg/m^3) during December 2016.~~ These quantitative estimations ~~suggest~~ demonstrate that ~~the ABL anomaly to a large extent explains~~ the ~~enhanced~~ elevated $PM_{2.5}$ concentrations during ~~these~~ the three polluted months can be largely attributed to anomalous ABL conditions.

Table 1. Estimated contribution of ABL anomaly to elevated $PM_{2.5}$ concentration in January of 2013, December of 2015 and December of 2016.

Pollution month	Month-averaged $PM_{2.5}$ concentration (μg/m^3)	Total anomaly C' (μg/m^3)	ABL-driven anomaly C_{ABL}' (μg/m^3)	Contribution ratio of ABL-driven anomaly (%)
January 2013	180.1	76.1	44.4	58.3
December 2015	151.8	47.8	22.2	46.4
December 2016	151.2	47.2	34.6	73.3

4. Summary

The influence of ~~the~~ ABL ~~structure~~ meteorology on Beijing's air quality ~~is still~~is relatively unclear due to the lack of long-term observations. ~~On the other hand~~Meanwhile, the long years of routine radiosondes remain underutilized as a tool for urban pollution studies. In this study, the SOM was applied to ~~4~~5-year (2013-2017) radiosonde-based θ_v profiles~~s~~ to classify the state of ABL ~~types~~ over Beijing. The ~~resulting~~ classified ABL types were then evaluated in relation to ~~meteorological and environmental~~near-surface air quality ~~variables~~, with an attempt to understand the roles of the ~~different~~ changing ABL ~~conditions~~ structure in ~~regulating the~~ air quality variation in Beijing. The main findings are as follows:

1) The SOM provides a continuum of nine ABL types (i.e., SOM nodes), and each ~~type~~ is characterized with distinct ~~boundary layer meteorological conditions (including~~ dynamic and thermodynamic conditions~~).~~ within the ABL. Node 1 represent a near neutral layer with the lowest θ_v gradient and the highest wind speed. Node 3 features a strong static stability in the upper ABL. In contrast, Node 9 and Node 7 respectively correspond to the moderate and strong static stability in the lower ABL.

2) The self-organized ABL types are capable of characterizing the influence of nocturnal mixing on near-surface pollutant loadings. From the near neutral (i.e., ~~node~~ Node 1) to strong stable ~~ABL types~~conditions (i.e., ~~node~~ Node 9), the ~~surface~~ average concentrations of ~~SO_2, NO_2, CO, PM_{10} and~~ $PM_{2.5}$, NO_2 and CO ~~on average~~ increased dramatically during all seasons except summer.~~increase approximately 120-220 %.~~ Meanwhile, t~~T~~he diurnal ~~evolutions~~ cycles of these pollutant species are strongly modulated by ~~by temperature inversions~~ABL dynamics. Although the modulation effect varies from season to season, the higher peak concentrations commonly occur under the more stable conditions.~~—~~ ~~While an elevated inversion enhances the afternoon baseline concentration, the surface inversion improves the evening concentration increment. In contrast, O_3 show an opposite variation in response to the ABL types.~~However, increasing stability has opposite effect on O_3, resulting in the lowest O_3 level in Node 9. For SO_2, the highest average concentrations are typically observed in Node 3. The pre-noon SO_2 peaks are more significant after a strong stable night.

~~3) Boundary layer evolution affects the near-surface observations of locally and remotely sourced pollutants in very different ways, causing a distinct difference in the diurnal variations of SO_2 and other pollutants (e.g., NO_2, CO, PM_{10} and $PM_{2.5}$). Comparing the CO/SO_2 ratios in different ABL types reveals that the local contribution increases with enhanced static stability near the ground, and it is the stable boundary layer stratification rather than weak surface wind that confines the regional contribution.~~

~~4) With the stabilizing ABL processes, the atmosphere column is more loaded with both fine- and coarse-mode particles. Node 3 (dominated by elevated inversion and high relative humidity) corresponds to the most severe columnar aerosol pollution, characterized by the highest optical depth (1.22) and volume concentration (0.30 $\mu m^3/\mu m^2$). The larger negative ARF at the surface (> 110 W/m^2) and positive ARF within the atmosphere (> 60 W/m^2) are associated with the three stable ABL types (i.e., nodes 3, 6 and 9), suggesting the possible~~

~~influence of a positive feedback loop for causing high surface aerosol concentrations.~~

~~5)~~ Analysis of three typical wintertime ~~pollution~~ pollution months (i.e., January 2013, December 2015 and December 2016) suggests that the ABL types are one of the primary drivers of day-to-day $PM_{2.5}$ variations in Beijing~~'s air quality~~. During the three pollution months, the ~~frequency~~ frequency of the ~~stable ABL types (e.g., n~~stable ABL types~~odes 3 and 9)~~ (i.e., Nodes 9 and 3) increases~~s~~ significantly compared ~~with~~ to the ~~4~~5-year (2013-~~2016~~2017) winter mean~~ frequency~~. ~~In contrast, the frequency of the well-mixed ABL type (i.e., node 1) is greatly reduced during these pollution months.~~

~~6)~~3) Using a meteorology-to-environment method, the relative (absolute) contributions of the ABL anomaly to ~~enhanced~~ elevated $PM_{2.5}$ ~~level~~ concentrations ~~is~~ are estimated to be ~~65~~58.~~8~~3 % (~~46~~44.~~2~~4 μg/m^3) ~~during~~ in January 2013, 46.~~7~~4 % (~~20~~22.2 μg/m^3) ~~during~~ in December 2015, and ~~94~~73.~~6~~3 % (~~35~~34.~~3~~6 μg/m^3) ~~during~~ in December 2016.

This work revealed the common pattern of the ABL influences ~~of different ABL structures~~ on Beijing' air quality. The established ~~correlations~~ linkages between ABL type and air quality could be useful for developing an operational forecast and warning system. In addition, this work demonstrated that the SOM-based ABL classification scheme is a ~~powerful~~ helpful tool for understanding urban air pollution. Since the SOM technique is good at ~~feather~~feature extraction, the coarse-resolution radiosonde~~ profile~~s can be taken as ~~the SOM~~ input ~~(as we have shown in this study)~~to classify the state of the ABL. Therefore, the SOM-based ABL classification scheme~~it~~ can take advantage of the long-term available radiosondes, ~~which is~~making it a simple and economical alternative to ~~to implement in comparison to conventional~~other ~~techniques~~approaches to stability classification~~ (such as mooring boats, airplane, and ground remote sensing)~~. We believe that the pollution-related ABL research and the formulation of pollution control measures could benefit from application of the SOM analytical tool.

Data availability

The datasets used in this study are publicly available at the University of Wyoming (http://weather.uwyo.edu/), the Ministry of Environmental Protection of the People's Republic of China (http://datacenter.mep.gov.cn/), the U.S. Department of State Air Quality Monitoring Program (http://www.stateair.net/)~~, and the Aerosol Robotic Network (https://aeronet.gsfc.nasa.gov/)~~.

Competing interests

The authors declare no conflict of interest.

Acknowledgements

This study is supported by the National Key Research and Development Plan of China (Nos. 2017YFC0209606 and 2016YFC0203305), the National Natural Science Foundation of China (Nos. 41630422, 41475140 and 41475004) and the Special Fund for Basic Scientific Research Business of Central Public Research Institutes (PM-zx703-201601-019). The authors would like to thank the Beijing Meteorological Bureau, the Ministry of Environmental Protection of the People's Republic of China and the Wyoming Weather Web for providing related data. ~~Concerning the AERONET data used in this paper, we are particularly grateful to Prof. Huizheng Che, Prof. Hongbin Chen and Prof. Philippe Goloub for their efforts in establishing and maintaining the AERONET site in Beijing, as well as their assistants for the upkeep of the instrument and availability of the online data.~~

References

Cai, W. J., Li, K., Liao, H., Wang, H. J., and Wu, L. X.: Weather conditions conducive to Beijing severe haze more frequent under climate change, Nat Clim Change, 7, 257-+, 10.1038/Nclimate3249, 2017.

Chambers, S. D., Wang, F. J., Williams, A. G., Deng, X. D., Zhang, H., Lonati, G., Crawford, J., Griffiths, A. D., Ianniello, A., and Allegrini, I.: Quantifying the influences of atmospheric stability on air pollution in Lanzhou, China, using a radon-based stability monitor, Atmos Environ, 107, 233-243, 10.1016/j.atmosenv.2015.02.016, 2015a.

Chambers, S. D., Williams, A. G., Crawford, J., and Griffiths, A. D.: On the use of radon for quantifying the effects of atmospheric stability on urban emissions, Atmos Chem Phys, 15, 1175-1190, 10.5194/acp-15-1175-2015, 2015b.

Chen, L. W. A., Watson, J. G., Chow, J. C., Green, M. C., Inouye, D., and Dick, K.: Wintertime particulate pollution episodes in an urban valley of the Western US: a case study, Atmos Chem Phys, 12, 10051-10064, 10.5194/acp-12-10051-2012, 2012.

Chen, Y., Zhao, C. S., Zhang, Q., Deng, Z. Z., Huang, M. Y., and Ma, X. C.: Aircraft study of Mountain Chimney Effect of Beijing, China, J Geophys Res-Atmos, 114, Artn D08306
10.1029/2008jd010610, 2009.

Chen, Z. H., Cheng, S. Y., Li, J. B., Guo, X. R., Wang, W. H., and Chen, D. S.: Relationship between atmospheric pollution processes and synoptic pressure patterns in northern China, Atmos Environ, 42, 6078-6087, 10.1016/j.atmosenv.2008.03.043, 2008.

Dyson, L. L.: A heavy rainfall sounding climatology over Gauteng, South Africa, using self-organising maps, Clim Dynam, 45, 3051-3065, 10.1007/s00382-015-2523-3, 2015.

Fan, S. J., Wang, B. M., Tesche, M., Engelmann, R., Althausen, A., Liu, J., Zhu, W., Fan, Q., Li, M. H., Ta, N., Song, L. L., and Leong, K. C.: Meteorological conditions and structures of atmospheric boundary layer in October 2004 over Pearl River Delta area, Atmos Environ, 42, 6174-6186, 10.1016/j.atmosenv.2008.01.067, 2008.

Gao, M., Guttikunda, S. K., Carmichael, G. R., Wang, Y. S., Liu, Z. R., Stanier, C. O., Saide, P. E., and Yu, M.: Health impacts and economic losses assessment of the 2013 severe haze event in Beijing area, Sci Total Environ, 511, 553-561, 10.1016/j.scitotenv.2015.01.005, 2015.

Gao, M., Carmichael, G. R., Wang, Y., Saide, P. E., Yu, M., Xin, J., Liu, Z., and Wang, Z.: Modeling study of the 2010 regional haze event in the North China Plain, Atmos Chem Phys, 16, 1673-1691, 10.5194/acp-16-1673-2016, 2016.

Gao, M., Saide, P. E., Xin, J. Y., Wang, Y. S., Liu, Z. R., Wang, Y. X., Wang, Z. F., Pagowski, M., Guttikunda, S. K., and Carmichael, G. R.: Estimates of Health Impacts and Radiative Forcing in Winter Haze in Eastern China through Constraints of Surface PM2.5 Predictions, Environ Sci Technol, 51, 2178-2185, 10.1021/acs.est.6b03745, 2017.

Gibson, P. B., Perkins-Kirkpatrick, S. E., and Renwick, J. A.: Projected changes in synoptic weather patterns over New Zealand examined through self-organizing maps, Int J Climatol, 36, 3934-3948, 10.1002/joc.4604, 2016.

Guinot, B., Roger, J. C., Cachier, H., Wang, P. C., Bai, J. H., and Tong, Y.: Impact of vertical atmospheric structure on Beijing aerosol distribution, Atmos Environ, 40, 5167-5180, 10.1016/j.atmosenv.2006.03.051, 2006.

Guo, J. P., Miao, Y. C., Zhang, Y., Liu, H., Li, Z. Q., Zhang, W. C., He, J., Lou, M. Y., Yan, Y., Bian, L. G., and Zhai, P.: The climatology of planetary boundary layer height in China derived from radiosonde and reanalysis data, Atmos Chem Phys, 16, 13309-13319, 10.5194/acp-16-13309-2016, 2016.

Guo, X. F., Yang, T., Miao, S. G., and Sun, Y. L.: Urban Boundary-Layer Stability and Turbulent Exchange during Consecutive Episodes of Particle Air Pollution in Beijing, China, Atmospheric and Oceanic Science Letters, 7, 62-66, 10.3878/j.issn.1674-2834.13.0067, 2014.

Holzworth, G. C.: Estimates of mean maximun mixing depths in the contiguous United States, Monthly Weather Review, 92, 235-242, 1964.

Holzworth, G. C.: Mixing depths, wind speeds and air pollution potential for selected locations in the United States, J Appl Meteorol, 6, 1039-1044, 1967.

Hu, X. M., Ma, Z. Q., Lin, W. L., Zhang, H. L., Hu, J. L., Wang, Y., Xu, X. B., Fuentes, J. D., and Xue, M.: Impact of the Loess Plateau on the atmospheric boundary layer structure and air quality in the North China Plain: A case study, Sci Total Environ, 499, 228-237, 10.1016/j.scitotenv.2014.08.053, 2014.

Hua, Y., Wang, S., Wang, J., Jiang, J., Zhang, T., Song, Y., Kang, L., Zhou, W., Cai, R., Wu, D., Fan, S., Wang, T., Tang, X., Wei, Q., Sun, F., and Xiao, Z.: Investigating the impact of regional transport on PM2.5 formation using vertical observation during APEC 2014 Summit in Beijing, Atmos Chem Phys, 16, 15451-15460, 10.5194/acp-16-15451-2016, 2016.

Jensen, A. A., Thompson, A. M., and Schmidlin, F. J.: Classification of Ascension Island and Natal ozonesondes using self-organizing maps, J Geophys Res-Atmos, 117, Artn D04302
10.1029/2011jd016573, 2012.

Ji, D. S., Wang, Y. S., Wang, L. L., Chen, L. F., Hu, B., Tang, G. Q., Xin, J. Y., Song, T., Wen, T. X., Sun, Y., Pan, Y. P., and Liu, Z. R.: Analysis of heavy pollution episodes in selected cities of northern China, Atmos Environ, 50, 338-348, 10.1016/j.atmosenv.2011.11.053, 2012.

Jiang, N. B., Scorgie, Y., Hart, M., Riley, M. L., Crawford, J., Beggs, P. J., Edwards, G. C., Chang, L. S., Salter, D., and Virgilio, G. D.: Visualising the relationships between synoptic circulation type and air quality in Sydney, a subtropical coastal-basin environment, Int J Climatol, 37, 1211-1228, 10.1002/joc.4770, 2017.

Katurji, M., Noonan, B., Zawar-Reza, P., Schulmann, T., and Sturman, A.: Characteristics of the Springtime Alpine Valley Atmospheric Boundary Layer Using Self-Organizing Maps, J Appl Meteorol Clim, 54, 2077-2085, 10.1175/Jamc-D-14-0317.1, 2015.

Kaufman, Y. J., Tanre, D., and Boucher, O.: A satellite view of aerosols in the climate system, Nature, 419, 215-223, 10.1038/nature01091, 2002.

Kohonen, T.: Self-organized information of topologically correct features maps, Biological Cybernetics 43, 59-69, 1982.

Kohonen, T.: Self-organizing maps, 3rd edn. Springer, London, 2001.

Lennard, C., and Hegerl, G.: Relating changes in synoptic circulation to the surface rainfall response using self-organising maps, Clim Dynam, 44, 861-879, 10.1007/s00382-014-2169-6, 2015.

Li, Y. Y., Yan, J. P., and Sui, X. B.: Tropospheric temperature inversion over central China, Atmos Res, 116, 105-115, 10.1016/j.atmosres.2012.03.009, 2012.

Liao, J. W., Jin, A. Z., Chafe, Z. A., Pillarisetti, A., Yu, T., Shan, M., Yang, X. D., Li, H. X., Liu, G. Q., and Smith, K. R.: The impact of household cooking and heating with solid fuels on ambient PM2.5 in peri-urban Beijing, Atmos Environ, 165, 62-72, 10.1016/j.atmosenv.2017.05.053, 2017.

Liu, H. Z., Feng, J. W., Jarvi, L., and Vesala, T.: Four-year (2006-2009) eddy covariance measurements of CO2 flux over an urban area in Beijing, Atmos Chem Phys, 12, 7881-7892, 10.5194/acp-12-7881-2012, 2012.

Liu, Y. G., Weisberg, R. H., and Mooers, C. N. K.: Performance evaluation of the self-organizing map for feature extraction, J Geophys Res-Oceans, 111, Artn C05018
10.1029/2005jc003117, 2006.

Miao, Y., Guo, J., Liu, S., Liu, H., Li, Z., Zhang, W., and Zhai, P.: Classification of summertime synoptic patterns in Beijing and their associations with boundary layer structure affecting aerosol pollution, Atmos Chem Phys, 17, 3097-3110, 10.5194/acp-17-3097-2017, 2017.

Pearce, J. L., Waller, L. A., Chang, H. H., Klein, M., Mulholland, J. A., Sarnat, J. A., Sarnat, S. E., Strickland, M. J., and Tolbert, P. E.: Using self-organizing maps to develop ambient air quality classifications: a time series example, Environ Health-Glob, 13, 10.1186/1476-069X-13-56, 2014.

Platis, A., Altstadter, B., Wehner, B., Wildmann, N., Lampert, A., Hermann, M., Birmili, W., and Bange, J.: An Observational Case Study on the Influence of Atmospheric Boundary-Layer Dynamics on New Particle Formation, Bound-Lay Meteorol, 158, 67-92, 10.1007/s10546-015-0084-y, 2016.

Quan, J. N., Gao, Y., Zhang, Q., Tie, X. X., Cao, J. J., Han, S. Q., Meng, J. W., Chen, P. F., and Zhao, D. L.: Evolution of planetary boundary layer under different weather conditions, and its impact on aerosol concentrations, Particuology, 11, 34-40, 10.1016/j.partic.2012.04.005, 2013.

Salmond, J. A., and McKendry, I. G.: A review of turbulence in the very stable nocturnal boundary layer and its implications for air quality, Progress in Physical Geography, 29, 171-188, 10.1191/0309133305pp442ra, 2005.

Stauffer, R. M., Thompson, A. M., and Young, G. S.: Tropospheric ozonesonde profiles at long-term US monitoring sites: 1. A climatology based on self-organizing maps, J Geophys Res-Atmos, 121, 1320-1339, 10.1002/2015JD023641, 2016.

Stull, R. B.: An Introduction to Boundary Layer Meteorology. Kluwer, 1988.

Sun, Y., Song, T., Tang, G. Q., and Wang, Y. S.: The vertical distribution of PM2.5 and boundary-layer structure during summer haze in Beijing, Atmos Environ, 74, 413-421, 10.1016/j.atmosenv.2013.03.011, 2013.

Sun, Y. L., Du, W., Wan, Q. Q., Zhang, Q., Chen, C., Chen, Y., Chen, Z. Y., Fu, P. Q., Wang, Z. F., Gao, Z. Q., and Worsnop, D. R.: Real-Time Characterization of Aerosol Particle Composition above the Urban Canopy in Beijing: Insights into the Interactions between the Atmospheric Boundary Layer and Aerosol Chemistry, Environ Sci Technol, 49, 11340-11347, 10.1021/acs.est.5b02373, 2015.

Tang, G., Zhu, X., Hu, B., Xin, J., Wang, L., Munkel, C., Mao, G., and Wang, Y.: Impact of emission controls on air quality in Beijing during APEC 2014: lidar ceilometer observations, Atmos Chem Phys, 15, 12667-12680, 10.5194/acp-15-12667-2015, 2015.

Tang, G. Q., Zhang, J. Q., Zhu, X. W., Song, T., Munkel, C., Hu, B., Schafer, K., Liu, Z. R., Zhang, J. K., Wang, L. L., Xin, J. Y., Suppan, P., and Wang, Y. S.: Mixing layer height and its implications for air pollution over Beijing, China, Atmos Chem Phys, 16, 2459-2475, 10.5194/acp-16-2459-2016, 2016.

Tang, G. Q., Zhu, X. W., Xin, J. Y., Hu, B., Song, T., Sun, Y., Wang, L. L., Wu, F. K., Sun, J., Cheng, M. T., Chao, N., Li, X., and Wang, Y. S.: Modelling study of boundary-layer ozone over northern China - Part II: Responses to emission reductions during the Beijing Olympics, Atmos Res, 193, 83-93, 10.1016/j.atmosres.2017.02.014, 2017a.

Tang, G. Q., Zhu, X. W., Xin, J. Y., Hu, B., Song, T., Sun, Y., Zhang, J. Q., Wang, L. L., Cheng, M. T., Chao, N., Kong, L. B., Li, X., and Wang, Y. S.: Modelling study of boundary-layer ozone over northern China - Part I: Ozone budget in summer, Atmos Res, 187, 128-137, 10.1016/j.atmosres.2016.10.017, 2017b.

Whiteman, C. D., Hoch, S. W., Horel, J. D., and Charland, A.: Relationship between particulate air pollution and meteorological variables in Utah's Salt Lake Valley, Atmos Environ, 94, 742-753, 10.1016/j.atmosenv.2014.06.012, 2014.

Wolf, T., Esau, I., and Reuder, J.: Analysis of the vertical temperature structure in the Bergen valley, Norway, and its connection to pollution episodes, J Geophys Res-Atmos, 119, 10645-10662, 10.1002/2014JD022085, 2014.

Wu, M., Wu, D., Fan, Q., Wang, B. M., Li, H. W., and Fan, S. J.: Observational studies of the meteorological characteristics associated with poor air quality over the Pearl River Delta in China, Atmos Chem Phys, 13, 10755-10766, 10.5194/acp-13-10755-2013, 2013.

Xu, W. Y., Zhao, C. S., Ran, L., Lin, W. L., Yan, P., and Xu, X. B.: SO2 noontime-peak phenomenon in the North China Plain, Atmos Chem Phys, 14, 7757-7768, 10.5194/acp-14-7757-2014, 2014.

Xu, X., Zhao, T., Liu, F., Gong, S. L., Kristovich, D., Lu, C., Guo, Y., Cheng, X., Wang, Y., and Ding, G.: Climate modulation of the Tibetan Plateau on haze in China, Atmos Chem Phys, 16, 1365-1375, 10.5194/acp-16-1365-2016, 2016.

Ye, X. X., Song, Y., Cai, X. H., and Zhang, H. S.: Study on the synoptic flow patterns and boundary layer process of the severe haze events over the North China Plain in January 2013, Atmos Environ, 124, 129-145, 10.1016/j.atmosenv.2015.06.011, 2016.

Zhang, J. K., Sun, Y., Liu, Z. R., Ji, D. S., Hu, B., Liu, Q., and Wang, Y. S.: Characterization of submicron aerosols during a month of serious pollution in Beijing, 2013, Atmos Chem Phys, 14, 2887-2903, 10.5194/acp-14-2887-2014, 2014.

Zhang, J. P., Zhu, T., Zhang, Q. H., Li, C. C., Shu, H. L., Ying, Y., Dai, Z. P., Wang, X., Liu, X. Y., Liang, A. M., Shen, H. X., and Yi, B. Q.: The impact of circulation patterns on regional transport pathways and air quality over Beijing and its surroundings, Atmos Chem Phys, 12, 5031-5053, 10.5194/acp-12-5031-2012, 2012.

Zhang, Q., Ma, X. C., Tie, X. X., Huang, M. Y., and Zhao, C. S.: Vertical distributions of aerosols under different weather conditions: Analysis of in-situ aircraft measurements in Beijing, China, Atmos Environ, 43, 5526-5535, 10.1016/j.atmosenv.2009.05.037, 2009.

Zhao, B., Wang, P., Ma, J. Z., Zhu, S., Pozzer, A., and Li, W.: A high-resolution emission inventory of primary pollutants for the Huabei region, China, Atmos Chem Phys, 12, 481-501, 10.5194/acp-12-481-2012, 2012.

Zhao, X. J., Zhao, P. S., Xu, J., Meng, W., Pu, W. W., Dong, F., He, D., and Shi, Q. F.: Analysis of a winter regional haze event and its formation mechanism in the North China Plain, Atmos Chem Phys, 13, 5685-5696, 10.5194/acp-13-5685-2013, 2013.

Zhu, X. W., Tang, G. Q., Hu, B., Wang, L. L., Xin, J. Y., Zhang, J. K., Liu, Z. R., Munkel, C., and Wang, Y. S.: Regional pollution and its formation mechanism over North China Plain: A case study with ceilometer observations and model simulations, J Geophys Res-Atmos, 121, 14574-14588, 10.1002/2016JD025730, 2016.

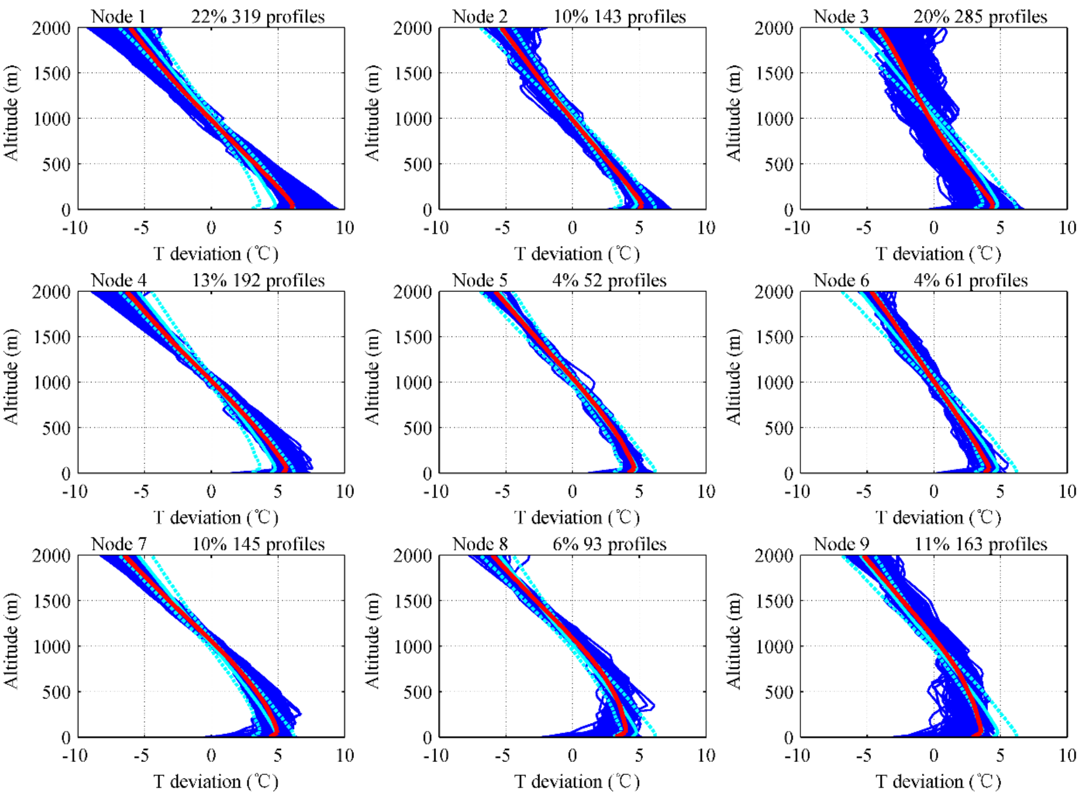

~~**Figure 1. The 3 × 3 SOM output for radiosonde-based temperature (T) deviation profiles observed at the Beijing Observatory. SOM nodes are shown in red, with the corresponding individual profiles in dark blue. For reference, the overall average temperature profile and 25th and 75th percentile profiles are shown in cyan. The top-right shows the occurrence cases and frequency of each SOM node.**~~

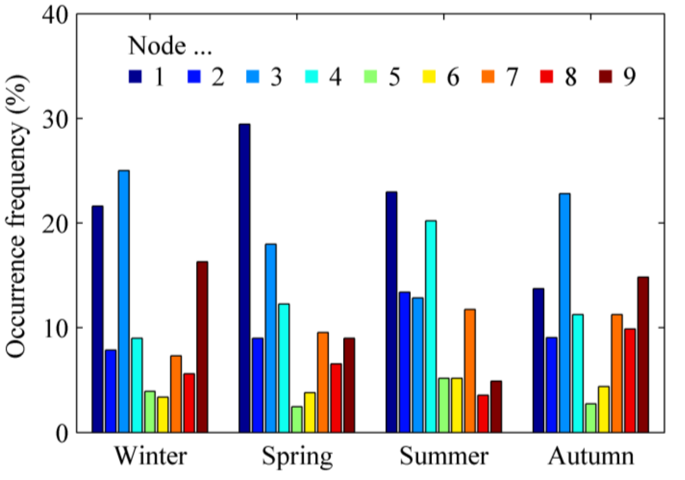

~~**Figure 2. Seasonality of SOM nodes shown as the relative frequency of seasons within each SOM node. Winter (DJF); Spring (MAM); Summer (JJA); Autumn (SON).**~~

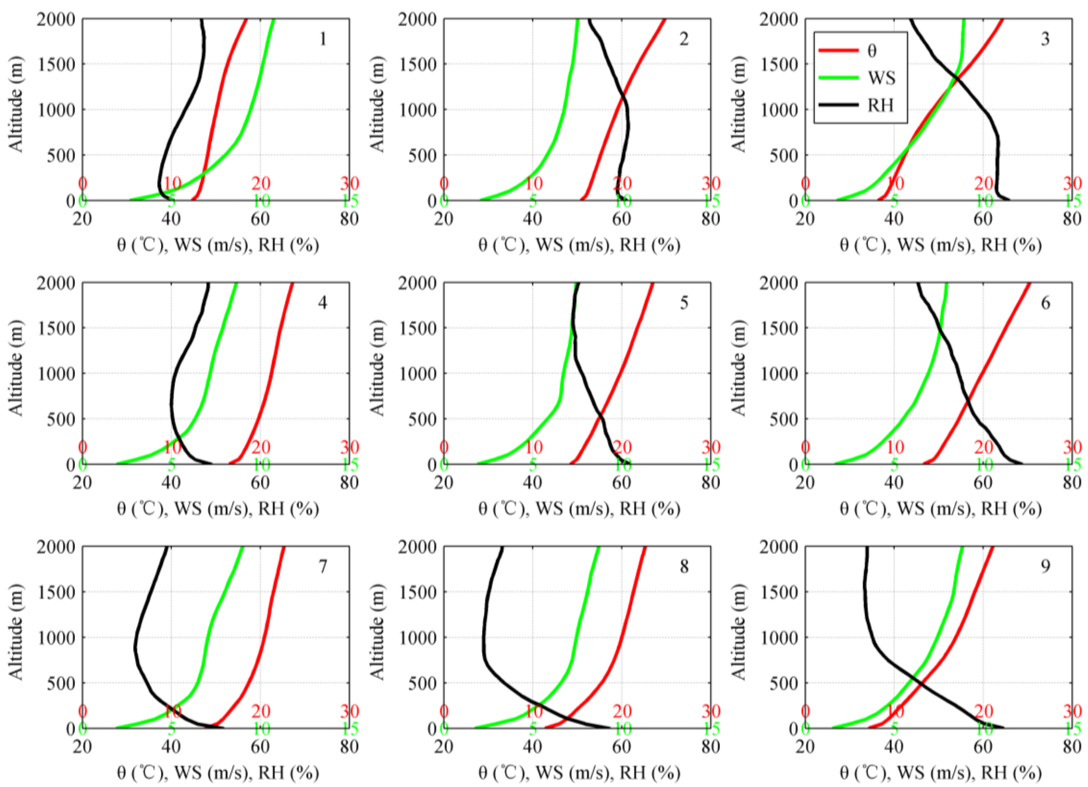

~~**Figure 3. Profiles of average potential temperature (θ), wind speed (WS) and relative humidity (RH) corresponding to each SOM node at the Beijing Observatory. The red, green and black labels of the horizontal axis correspond to θ, WS and RH, respectively.**~~

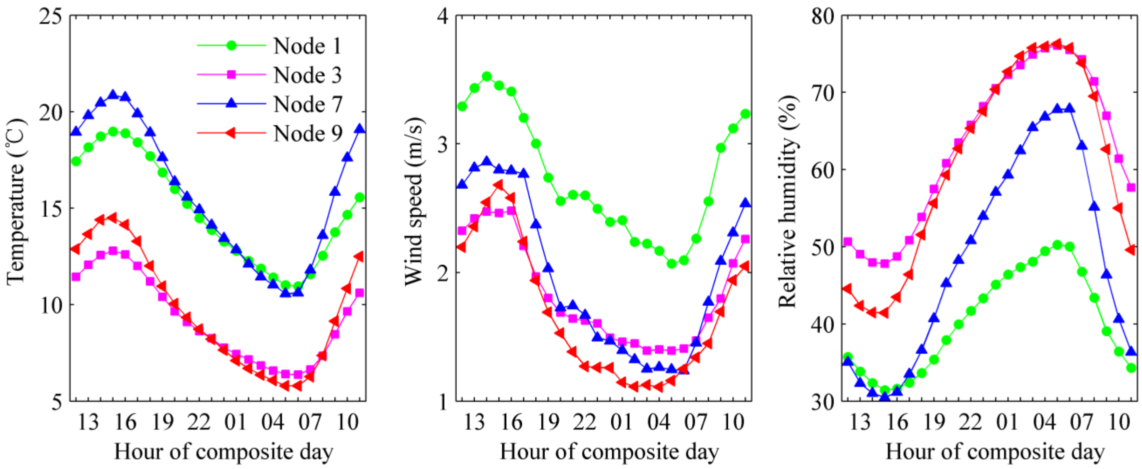

~~**Figure 4. Hourly mean diurnal composites of temperature, wind speed and relative humidity in Beijing corresponding to SOM nodes 1, 3, 7 and 9.**~~

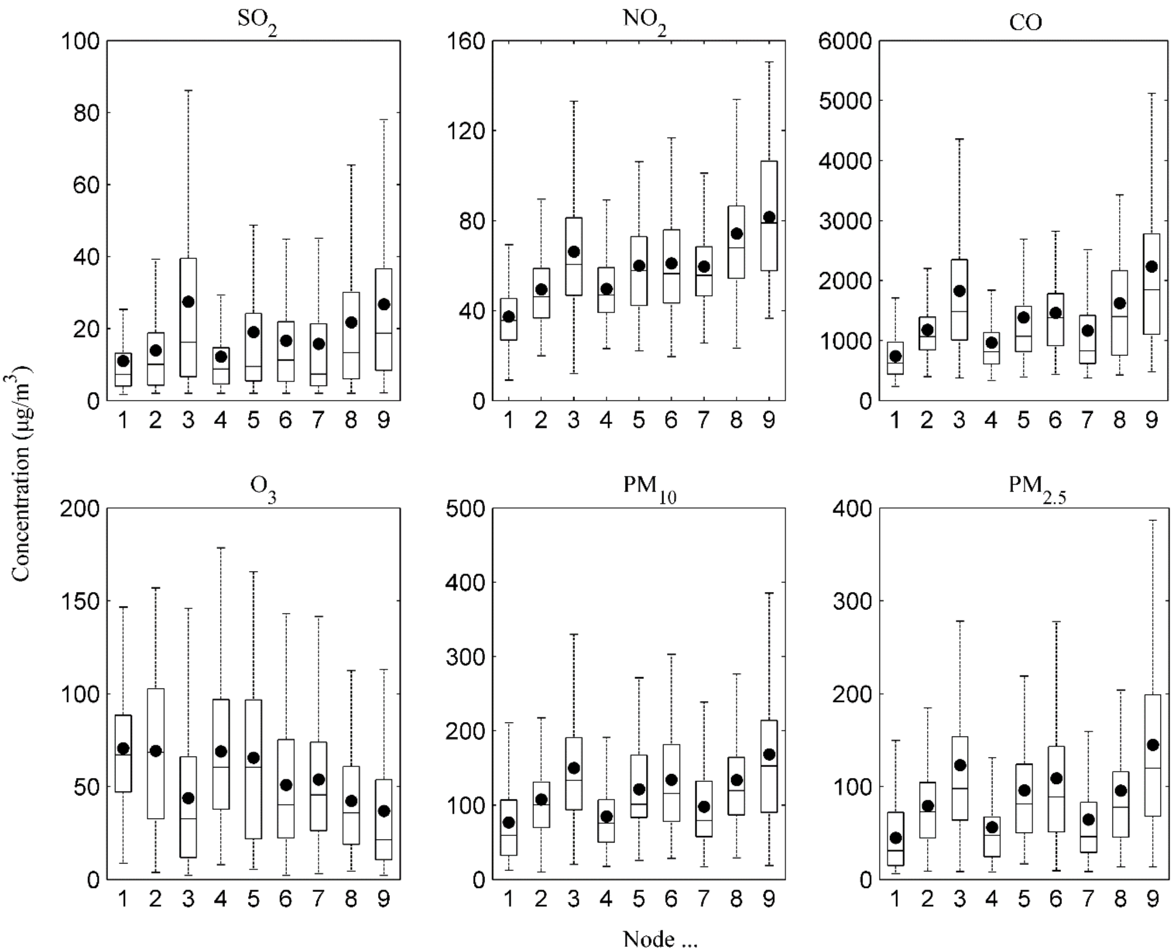

~~**Figure 5. Daily pollutant concentrations in Beijing corresponding to each SOM node.**~~

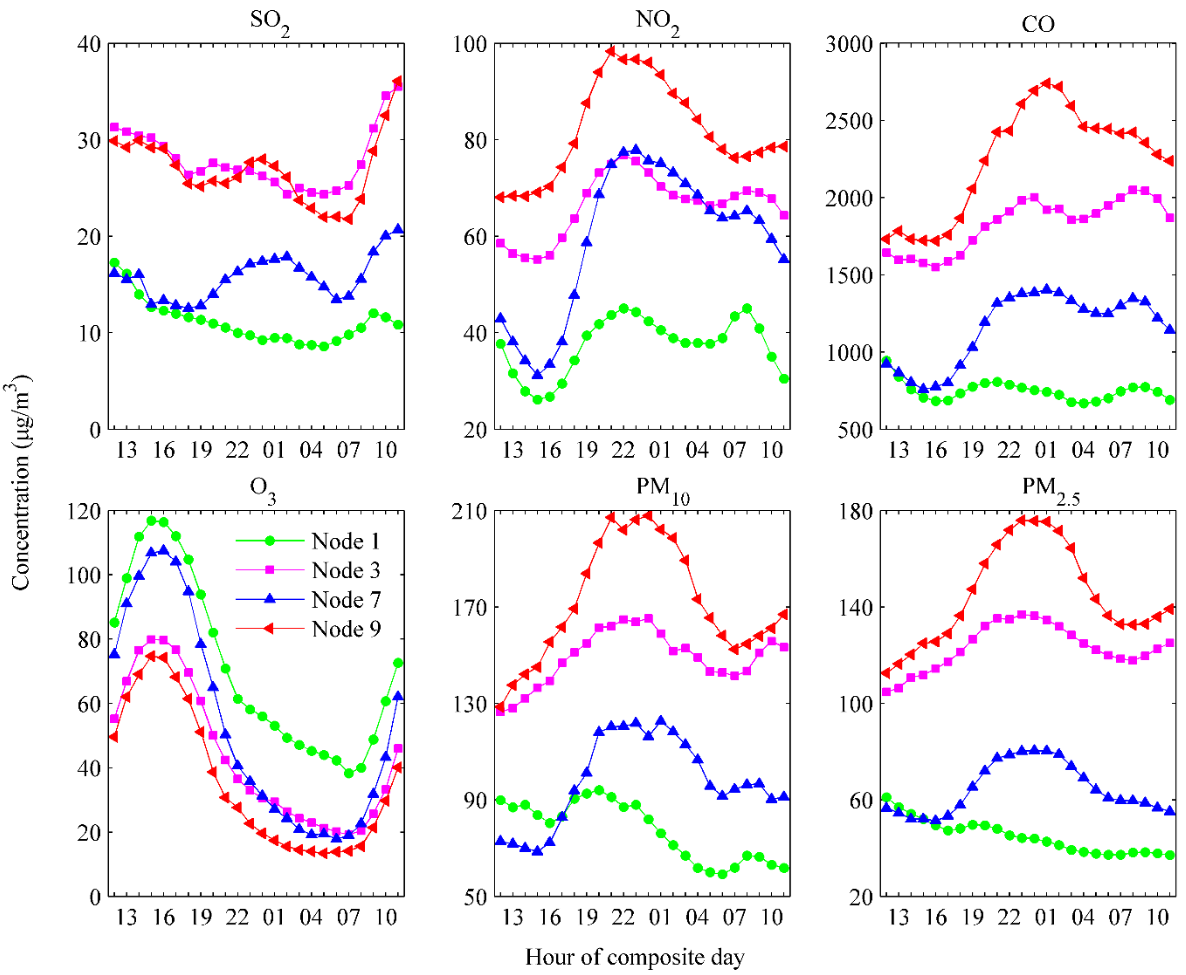

~~**Figure 6. Composite diurnal variations of air pollutants in Beijing corresponding to SOM nodes 1, 3, 7 and 9.**~~

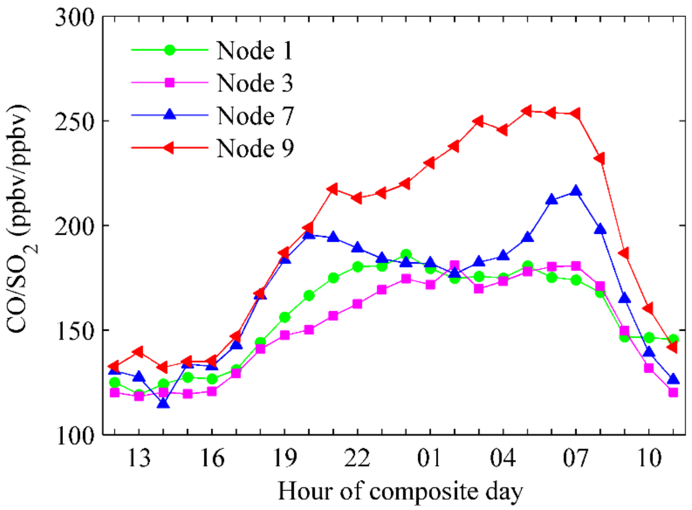

~~**Figure 7. Composite diurnal variations of CO/SO_2 ratios in Beijing corresponding to SOM nodes 1, 3, 7 and 9.**~~

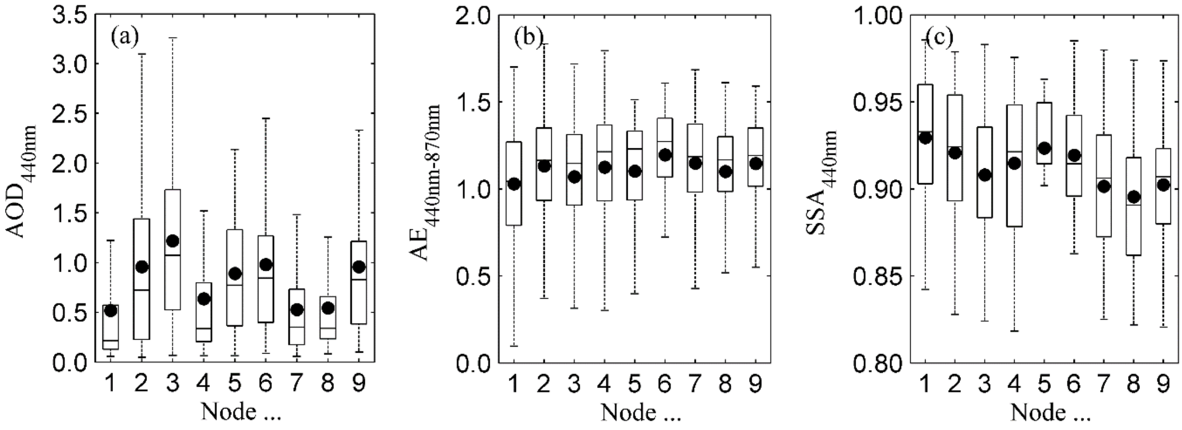

~~**Figure 8. (a) Aerosol optical depth (AOD_{440nm}), (b) Ångström exponent ($AE_{440nm-870nm}$) and (c) single scattering albedo (SSA_{440nm}) over Beijing and corresponding to each SOM node. The solid dots denote the mean. The box and whisker plot presents the median, the first and third quartiles, and the 5th and 95th percentiles, respectively.**~~

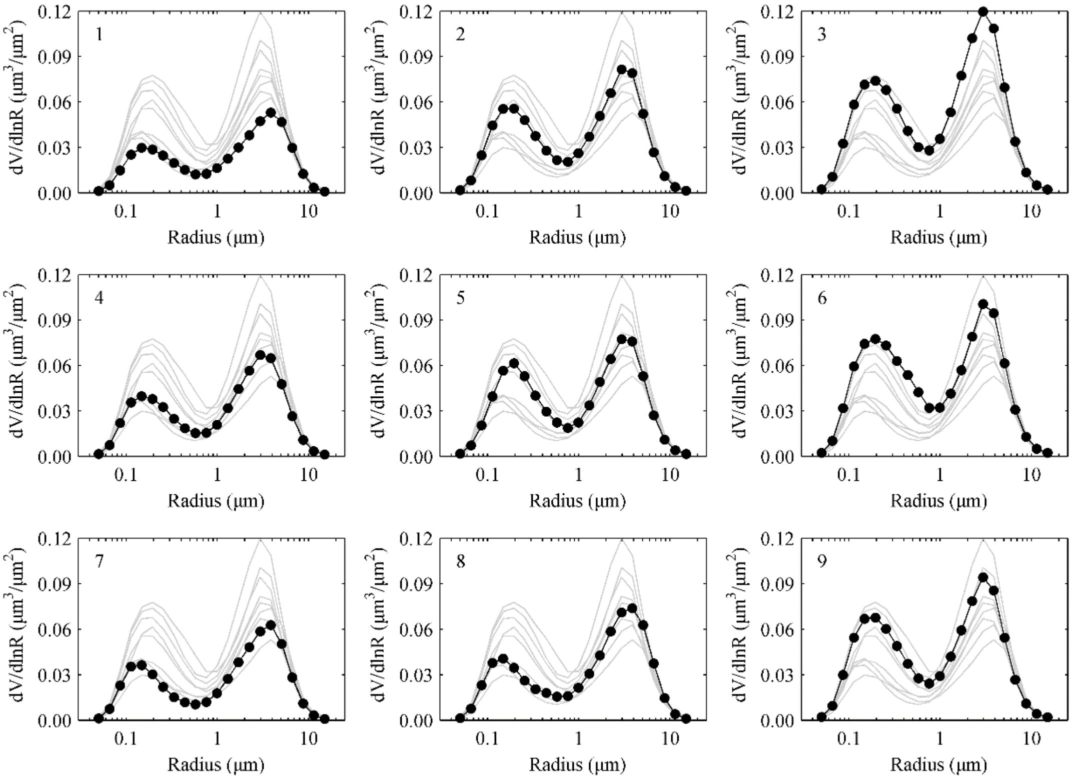

~~**Figure 9. Mean volume particle size distribution over Beijing corresponding to each SOM node. The average volume particle size distribution for each node is shown by the gray line and is repeated on each plot for comparison. The size distribution for each type is highlighted in the black dotted line on the respective plot.**~~

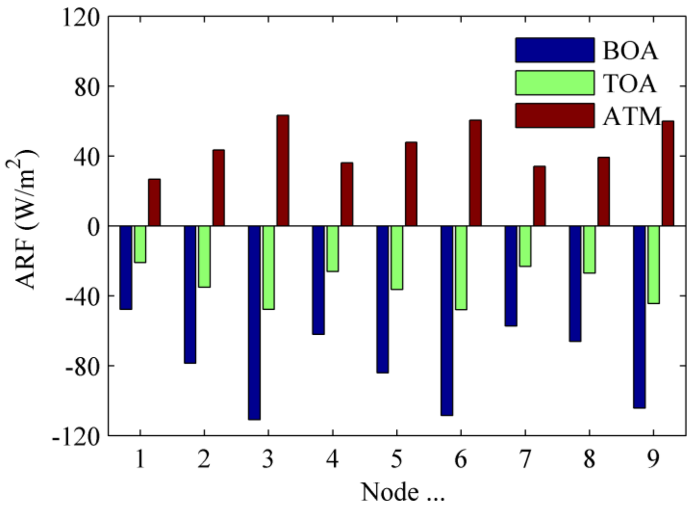

~~**Figure 10. Aerosol radiative forcing (ARF) at the surface (BOA), top of atmosphere (TOA), and within the atmosphere (ATM) over Beijing and corresponding to each SOM node.**~~

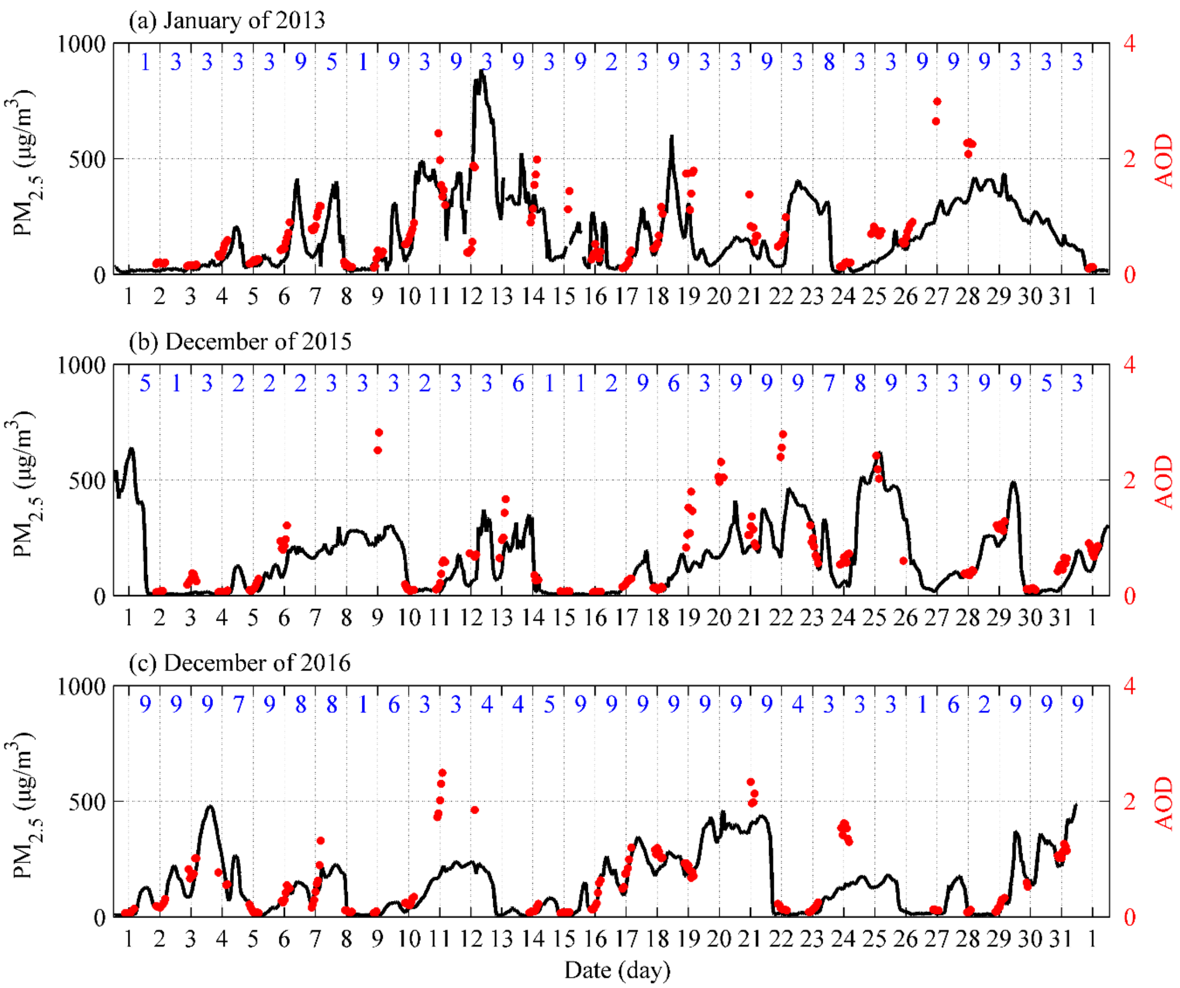

~~**Figure 11. Time series of hourly $PM_{2.5}$ and AOD_{440nm} in (a) January of 2013, (b) December of 2015, and (c) December of 2016. The daily SOM nodes (i.e., ABL types) are shown at the top of each plot (blue numbers).**~~

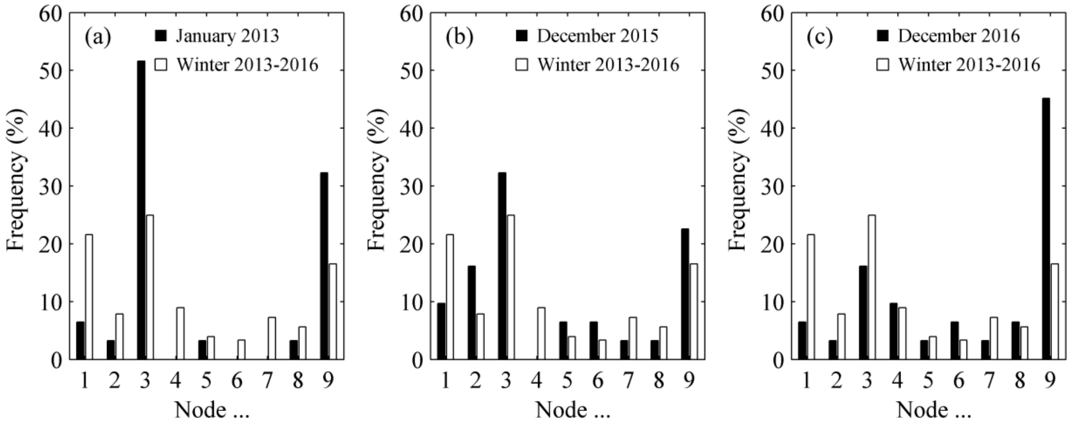

~~**Figure 12. Occurrence frequency of the SOM nodes during (a) January 2013, (b) December 2015, and (c) December 2016.**~~

~~Node …~~	~~Effective radius (μm)~~			~~Volume concentration ($\mu m^3/\mu m^2$)~~			~~*Vf/Vt*~~
	~~R_{eff}-T~~	~~R_{eff}-F~~	~~R_{eff}-C~~	~~VolCon-T~~	~~VolCon-F~~	~~VolCon-C~~	
~~1~~	~~0.54~~	~~0.14~~	~~2.46~~	~~0.13~~	~~0.05~~	~~0.09~~	~~0.31~~
~~2~~	~~0.41~~	~~0.16~~	~~2.42~~	~~0.21~~	~~0.09~~	~~0.12~~	~~0.42~~
~~3~~	~~0.45~~	~~0.16~~	~~2.30~~	~~0.30~~	~~0.12~~	~~0.18~~	~~0.41~~
~~4~~	~~0.45~~	~~0.15~~	~~2.38~~	~~0.17~~	~~0.06~~	~~0.11~~	~~0.36~~
~~5~~	~~0.47~~	~~0.17~~	~~2.44~~	~~0.21~~	~~0.09~~	~~0.12~~	~~0.41~~
~~6~~	~~0.38~~	~~0.17~~	~~2.33~~	~~0.28~~	~~0.14~~	~~0.14~~	~~0.45~~
~~7~~	~~0.42~~	~~0.14~~	~~2.37~~	~~0.15~~	~~0.05~~	~~0.10~~	~~0.34~~
~~8~~	~~0.44~~	~~0.14~~	~~2.32~~	~~0.18~~	~~0.06~~	~~0.12~~	~~0.35~~
~~9~~	~~0.38~~	~~0.16~~	~~2.25~~	~~0.25~~	~~0.11~~	~~0.14~~	~~0.43~~

~~**Table 1. Statistical parameters of aerosol particle size distribution corresponding to each SOM node. VolCon is the volume concentration; R_{eff} the effective radius; *Vf/Vt* denotes the fine-mode volume fraction. T, F, and C represent the total, fine-, and coarse-mode particles.**~~